arXiv:2501.06838v1 [eess.IV] 12 Jan 2025

# Generalized and Efficient 2D Gaussian Splatting for Arbitrary-scale Super-Resolution

Du Chen[1,2*] Liyi Chen[1*] Zhengqiang Zhang[1,2] Lei Zhang[1,2†]
[1]The Hong Kong Polytechnic University [2]OPPO Research Institute
{csdud.chen, liyi0308.chen, zhengqiang.zhang}@connet.polyu.hk, cslzhang@comp.polyu.edu.hk

## Abstract

*Equipped with the continuous representation capability of Multi-Layer Perceptron (MLP), Implicit Neural Representation (INR) has been successfully employed for Arbitrary-scale Super-Resolution (ASR). However, the limited receptive field of the linear layers in MLP restricts the representation capability of INR, while it is computationally expensive to query the MLP numerous times to render each pixel. Recently, Gaussian Splatting (GS) has shown its advantages over INR in both visual quality and rendering speed in 3D tasks, which motivates us to explore whether GS can be employed for the ASR task. However, directly applying GS to ASR is exceptionally challenging because the original GS is an optimization-based method through overfitting each single scene, while in ASR we aim to learn a single model that can generalize to different images and scaling factors. We overcome these challenges by developing two novel techniques. Firstly, to generalize GS for ASR, we elaborately design an architecture to predict the corresponding image-conditioned Gaussians of the input low-resolution image in a feed-forward manner. Secondly, we implement an efficient differentiable 2D GPU/CUDA-based scale-aware rasterization to render super-resolved images by sampling discrete RGB values from the predicted contiguous Gaussians. Via end-to-end training, our optimized network, namely GSASR, can perform ASR for any image and unseen scaling factors. Extensive experiments validate the effectiveness of our proposed method. The project page can be found at https://mt-cly.github.io/GSASR.github.io/.*

## 1. Introduction

Image Super-Resolution (SR) has been a challenging inverse problem in computer vision for many years, and a variety of deep learning-based (SR) methods have been developed in the past decade [5, 6, 39, 57, 61, 62, 65, 66, 70, 71, 73]. However, most of the existing SR models [9, 16, 37, 38, 60, 74, 77, 79, 80] are designed to operate only under integer or fixed scaling factors, *i.e.*, $\times 2$, $\times 3$, $\times 4$, due to the fact that they perform resolution upsampling by processing discrete pixels with de-convolutional layers [16] or pixel-shuffle layers [54]. As a result, it is hard for them to perform SR with decimal or even arbitrary scaling factors. Although the existing SR models could achieve arbitrary-scale zooming via adopting bicubic or bilinear interpolation, they would inevitably scarify image quality, leading to unsatisfied super-resolved results.

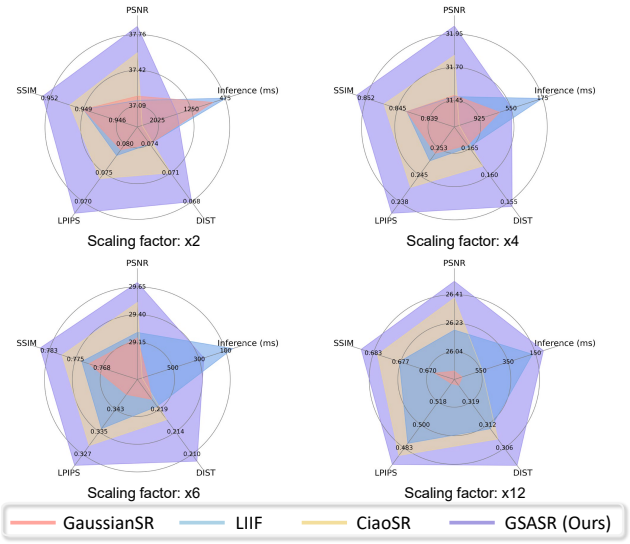


Figure 1. Comparison between GSASR and representative ASR methods on DIV2K. GSASR outperforms previous methods in visual quality with competitive inference time across both in-distribution ($\times 2$, $\times 4$) and out-of-distribution ($\times 6$, $\times 12$) scaling factors.

Inspired by the development of Implicit Neural Representation (INR) [48], Chen *et al*. presented LIIF [10] to address the problem of Arbitrary-scale SR (ASR) by making use of the continuity of Multi-Layer Perceptron (MLP) to query the RGB values of a high-resolution (HR) image and feeding its index to the MLP network. The following works

*Equal contribution.
†Corresponding author. This work is supported by the PolyU-OPPO Joint Innovative Research Center.

try to improve the ASR performance with local feature estimators [32] or scale-aware attention modules [2]. Most of the existing INR-based ASR models [2, 10, 32, 69] rely heavily on MLP layers to predict RGB pixels. However, this implicit function lacks enough representation capacity, as the linear layers in MLP have a very limited receptive field, which leads to limited reconstruction performance. Moreover, since the computations of different indices are usually unshared during the MLP feed-forward process, existing INR-based ASR methods have low computational efficiency and difficulties in scaling up the model parameters.

Recently, Gaussian Splatting (GS) [26] has shown its advantages over INR-based methods, such as Neural Radiance Field (NeRF) [48], in terms of both accuracy and complexity, thanks to its high computational efficiency and powerful explicit representation capabilities. GS has been successfully applied to tasks such as 3D reconstruction [4, 19], representation [18, 49], editing [11, 56], generation [12, 41], *etc*. While some studies have explored the use of GS for low-level vision tasks, *e.g*., image deblurring [8, 81], image compression [78], video super-resolution [68], these models overfit on the repetitive images from multi-frames in a video clip or multi-view cameras, or overfit on a single image to complete the image compression task. None of these methods could be applied to single image SR tasks, since overfitting a model on a single image cannot meet the generalization requirements of SR, where a single model should be used to super-resolve any input low-resolution (LR) image to its high-resolution (HR) counterpart.

Instead of overfitting the model to a fixed scenario, we switch from the optimization-based manner of original 3D GS [26] to a learning-based method and present **GSASR** (**G**aussian **S**platting based **A**rbitrary-scale **S**uper-**R**esolution), which adapts GS to the ASR task. Specifically, we first obtain the deep image features by encoding the input LR image with a general SR backbone [40, 79]. Secondly, inspired by DETR [3], we introduce learnable Gaussian embedding to output 2D Gaussians conditioned on the extracted image features. To enhance interaction among Gaussian embeddings, we perform window self-attention [42] for them so that they can adapt to each other. Then, the Gaussian embeddings are projected to predict the corresponding properties of 2D Gaussians, including the opacity, position, standard deviation, correlation coefficient, and peak RGB values. These 2D Gaussians depict the image in the contiguous Gaussian space. To render 2D Gaussians to obtain the super-resolved image with arbitrary scale, we implement an efficient differentiable GPU/CUDA-based rasterization, which receives the predicted 2D Gaussians with an upsampling scale vector as condition. The scale vector controls the sampling density, and all Gaussians are processed efficiently in parallel.

The advantages of our proposed GSASR are three-folds. (1) Due to the large receptive field brought by window-based self-attention modules, the Gaussian embeddings could sense long-range dependency from deep features and other embeddings. (2) The position of Gaussians are predicted explicitly, enabling Gaussians to concentrate on areas with complex textures, instead of being uniformly distributed over the whole image, thus leading to better reconstruction results. (3) Benefited from the developed efficient scale-aware 2D rasterization technique, GSASR is much faster than the state-of-the-art INR-based models. For example, under the scaling factor $\times 12$, GSASR could super-resolve an image to $720 \times 720$ resolution within only $91$ ms, while the state-of-the-art INR-based model such as CiaoSR [2] will cost nearly $540$ ms.

## 2. Related Work

SR aims to upscale the resolution of an LR input image. The community has witnessed a rapid development of SR methods, ranging from powerful feature extraction backbones [9, 13, 17, 21, 33, 35, 37, 38, 40, 47, 74, 77, 79, 80] to the utilization of generative models [5, 31, 34, 39, 43, 44, 51, 53, 57, 59–62, 65, 66, 70, 71, 73, 76] for better perceptual quality. While different methods differ from each other on specific designs, they all rely on upsampling operators to magnify the resolution of the original LR image. Various upsampling strategies have been developed, ranging from hand-crafted interpolation operators, to deep neural network-based convolutional layers [16, 54], and to implicit neural representations [10].

**Fixed-scale SR Methods**. In the early stage, deep neural network-based SR models [15, 27, 28, 30] usually adopt interpolation operators to magnify the resolution. They first upsample the resolution of an LR image to the size of its HR counterpart, and then feed it into network for detail enhancement. Such a scheme is straightforward but suffers from high computational cost. FSRCNN [16] is proposed to apply de-convolutional layers to upsample the resolution of the deep features at the end of the network, so as to accelerate the inference speed. ESPCN [54] performs upsampling by rearranging the LR feature maps into a higher-resolution space through pixel-shuffle layers. However, since the pixels are discrete in feature domain, the de-convolution or pixel-shuffle layers cannot perform continuous sampling to reconstruct SR images with arbitrary scales. Due to these limitations, most of the existing SR methods are conducted on integer scaling factors.

**Arbitrary-scale SR Methods**. The interpolation operators can be used to continuously predict neighborhood pixels at any magnification factors, yet they will sacrifice the image quality and obtain blurry results. Meta-SR [24] equips the network with the arbitrary-scale magnification ability by designing a meta-upscaling module that leverages DNN to predict HR details from LR neighborhood embeddings.

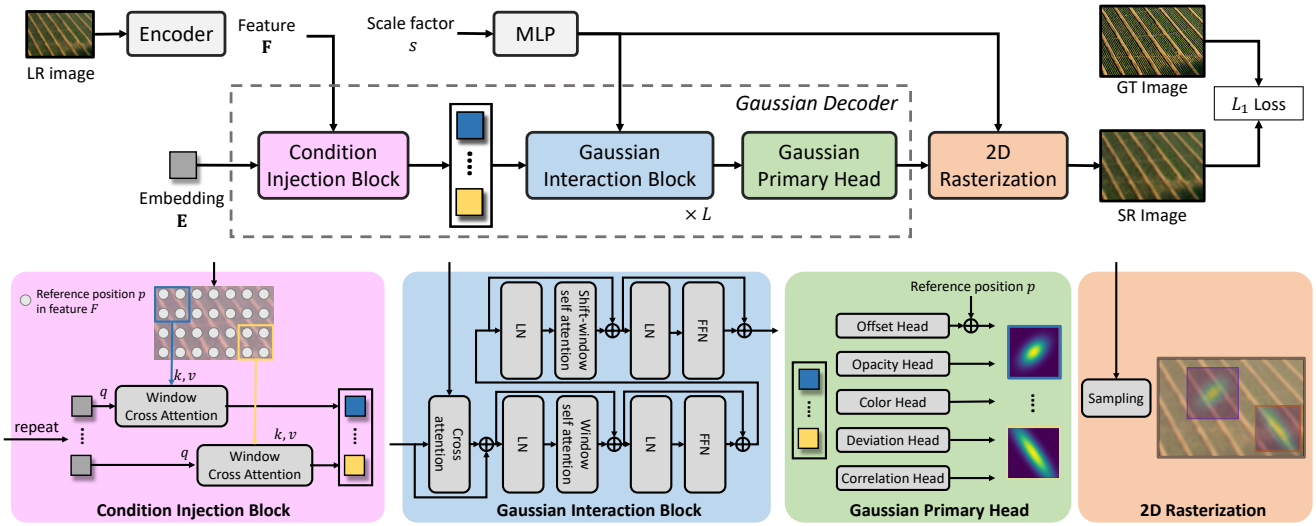


Figure 2. Overview of GSASR. In the training phase, an LR image is fed into the encoder to extract image features, conditioned on which the learnable Gaussian embeddings are passed through the Condition Injection Block and Gaussian Interaction Block to output 2D Gaussians. These 2D Gaussians are then rendered into an SR image of a specified resolution through differential rasterization.

Wang *et al*. [58] performed arbitrary upsampling by introducing dynamic filters generated based on the scaling factor. Inspired by the success of INR-based methods [48] in 3D tasks, LIIF [10] creatively introduces INR to complete the ASR task by learning an implicit mapping function between a pixel's RGB value and its index. Following LIIF, many INR-based models have been proposed. ITSRN [67] makes use of a transformer block and implicit position embedding to predict the super-resolved images. LTE [32] employs an implicit function to describe image features in Fourier domain. Based on Neural Operator [20], SRNO [64] adopts a kernel integral operator to fit the implicit function. BTC [50] employs B-spline implicit representation to achieve arbitrary-scale SR of screen content images. LINF [69] estimates a local implicit function with normalizing flow to model the naturalness of textures. CLIT [7] employs a cascaded cross-scale attention block with frequency encoding layers to sense neighborhood features. CiaoSR [2] introduces scale-aware attention-in-attention modules to extend the receptive field to promote the ASR performance. LMF [22] introduces a latent modulated function to compress the feature and accelerate the rendering process at the price of representation accuracy.

Very recently, GaussianSR [23] was proposed to employ GS for the ASR task. However, it has some significant drawbacks. Firstly, it only utilizes the position of RGB pixels from the low-resolution image to substite the center positions of Gaussians, heavily limiting the representation capability of Gaussians and leading to poor reconstruction performance. Secondly, it lacks a differentiable GPU/CUDA-based operator to complete the rasterization process, leading to low-efficiency and high computational cost. In contrast, our proposed GSASR predicts all of the parameters of Gaussians in an end-to-end manner, and we present an efficient differentiable 2D GPU/CUDA-based scare-aware rasterization to largely reduce the computational cost, leading to an effective and efficient model for accomplishing the ASR task.

## 3. Method

In this section, we first describe the concept and formulation of 2D Gaussian Spatting (GS), then present the model architecture and training details of our GSASR method.

### 3.1. 2D GS Representation and Rasterization

**2D GS Representation**. Our key insight is to represent an image using contiguous Gaussians, which can fit various frequency components of an image due to the powerful expressive properties of GS. Specifically, considering an LR image $I_{LR}$ of size $H \times W$, we represent it using $N$ 2D Gaussians, denoted by $\mathcal{G} = \{G_1, G_2, ..., G_N\}$. Each Gaussian maintains properties of opacity $\alpha \in [0,1]^1$, center position $\mu = \{\mu_x \in \mathbb{R}^1, \mu_y \in \mathbb{R}^1\}$, standard deviation $\sigma = \{\sigma_x \in (0,\infty)^1, \sigma_y \in (0,\infty)^1\}$, correlation coefficient $\rho \in [-1,1]^1$, and normalized peak RGB value $c \in [0,1]^3$. We define the color at position $(x,y)$ contributed by Gaussian $G$ as $G(x,y)$ (here we omit the index of Gaussians for simplicity of expression):

$$G(x,y) = \alpha \cdot c \cdot f(x,y). \tag{1}$$

The calculation of $f(x,y)$ is defined following typical 2D Gaussian distribution:

$$f(x,y) = e^{-\frac{1}{2(1-\rho^2)}(\frac{\Delta x^2}{\sigma_x^2} - \frac{2\rho\Delta x\Delta y}{\sigma_x\sigma_y} + \frac{\Delta y^2}{\sigma_y^2})}, \tag{2}$$

where $\Delta x = x - \mu_x$ and $\Delta y = y - \mu_y$. The color of the LR image at position $(x \in [0, W-1], y \in [0, H-1])$ is represented as the summarization of all $N$ Gaussians:

$$I_{LR}(x,y) = \sum_{i=1}^{N} G_i(x,y). \tag{3}$$

Gaussian functions are contiguous, enabling sampling at arbitrary positions. With a given scaling factor $s$, to obtain an SR image $I_{SR}$ of size $sH \times sW$, we sample the color at position $(x \in [0, sW-1], y \in [0, sH-1])$ with the following scale-aware rasterization:

$$I_{SR}(x,y;s) = \sum_{i=1}^{N} G_i(\frac{x}{s}, \frac{y}{s}). \tag{4}$$

**Fast Rasterization.** Simply rendering an SR image by querying each pixel from all 2D Gaussians leads to a complexity of $\mathcal{O}(s^2HWN)$, which is too high for high-resolution images. Actually, a Gaussian generally focuses on a limited area and its contribution to pixel values decays rapidly with the increase of distance. Therefore, we introduce a rasterization ratio $r < 1$ to control the rendering range of each Gaussian. Specifically, we handle all Gaussians in parallel and only render the pixels that are close enough to the Gaussian centers, greatly reducing the computational complexity to $\mathcal{O}(r^2s^2HWN)$ and making our algorithm practical. ($r$ is set to 0.1 in our implementation.) Note that our rasterization process is differential, which can be seamlessly integrated with neural networks for end-to-end optimization. Algorithm 1 describes the detailed steps of our scale-aware rasterization process. This algorithm is implemented via CUDA C++, which is GPU-friendly and achieves faster speed and low memory requirements.

**Algorithm 1:** 2D GS Scale-aware Rasterization

**Input:** $N$ 2D Gaussians $\{G_1, G_2, \ldots, G_N\}$; LR image of size $(H, W)$; scale factor $s$; rasterization ratio $r$.
**Output:** Rendered image $I_{SR}$

```
Initialize I_SR as an (sH, sW, 3) array of zeros.
For each G_i in {G_1, G_2, ..., G_N} do
    Initialize α, μ_x, μ_y, σ_x, σ_y, ρ, c from G_i.
    For each pixel (x, y) in I_SR do
        If |x − μ_x| < rsH and |y − μ_y| < rsW then
            Obtain f(x/s, y/s) using Eq. 2;
            Obtain G_i(x/s, y/s) using Eq. 1;
            I_SR(x, y; s) += G_i(x/s, y/s).
        end
    end
end
```

## 3.2. GSASR: Architecture and Modules

Conventional 3D Gaussian Splatting (GS) methods [26] directly optimize 3D Gaussians to fit a specific scene. As a result, they lack the generalization capability for the ASR tasks, where the model should be generalized to unseen images. To overcome this limitation, we introduce a novel network architecture, which conditions 2D Gaussians on low-resolution (LR) input images, generating content-aware Gaussian representations with enhanced generalization capabilities. Our proposed method, namely GSASR, is illustrated in Figure 2. It begins with an off-the-shelf encoder that extracts image features $\mathbf{F} \in \mathbb{R}^{H\times W\times C}$ from the LR input $\mathbf{I} \in \mathbb{R}^{H\times W\times 3}$, serving as input to the subsequent Gaussian generation process. The key of GSASR lies in the proposed *Gaussian decoder*, which receives image feature $\mathbf{F}$ and a learnable Gaussian embedding as inputs, and outputs 2D Gaussians $\mathcal{G}$ to depict the input image in contiguous Gaussian space. Our Gaussian decoder consists of *a condition injection block*, *a Gaussian interaction block*, and *a Gaussian primary head*. Finally, the output of Gaussian decoder is rasterized into the SR image.

**Gaussian Embedding.** In the GS decoder, we aim to represent the LR image through $N$ Gaussian embeddings $\mathbf{E} \in \mathbb{R}^{N\times d}$ conditioned on $\mathbf{F}$, where $d$ is the embedding dimension. A straightforward idea is to maintain $N$ independent learnable Gaussian embeddings that interact with image features to output $\mathcal{G}$. However, this approach suffers from both effectiveness and computational efficiency. First, the LR images exhibit variable sizes in the test phase. Rendering a fixed number of 2D Gaussians is inadequate to represent the details of a high-resolution LR image. Second, maintaining $N$ independent Gaussian embeddings not only introduces a significant memory burden but also faces optimization challenges, primarily attributed to the initial homogeneity and independent optimization of embeddings.

To address these limitations, we propose two key innovations. First, instead of setting a fixed value for $N$, we let $N$ be proportional to the LR image size ($N \propto H \times W$), employing more Gaussians to represent larger inputs. All Gaussian embeddings share the same initial weights, as shown in Figure 2. Second, to mitigate the optimization complexity and computational demands, inspired by Deform-DETR [82], we assign the $N$ Gaussian embeddings to different reference positions $p \in \mathbb{R}^{N\times 2}$ during initialization, which is obtained by sampling $N$ points at equal intervals from an $H \times W$ image. In this way, different Gaussian embeddings interpret the content at different regions based on their assigned reference positions, while they share the same weight initialization.

Table 1. Quantitative comparison between representative ASR models and our GSASR. All models use the same EDSR-backbone [40] as the feature extraction encoder. We test on DIV2K and LSDIR [36] datasets [55] with scaling factors ×2, ×3, ×4, ×6, ×8, ×12, ×16, ×18, ×24, ×30. The best results are highlighted in red. The PSNR and SSIM indices are computed in the Y channel of Ycbcr space.

| Scale | Metrics | Backbone: EDSR-baseline | | | | | | | | | | | | | | | | | |
|---|---|---|---|---|---|---|---|---|---|---|---|---|---|---|---|---|---|---|---|
| | | Testing Dataset: DIV2K | | | | | | | | | Testing Dataset: LSDIR | | | | | | | | |
| | | Meta -SR | LIIF | LTE | SRNO | LINF | LMF | Ciao -SR | Gaussian -SR | GSASR | Meta -SR | LIIF | LTE | SRNO | LINF | LMF | Ciao -SR | Gaussian -SR | GSASR |
| ×2 | PSNR | 36.02 | 36.05 | 36.10 | 36.27 | 36.21 | 36.21 | 36.42 | 36.10 | 36.65 | 31.36 | 31.43 | 31.50 | 31.65 | 31.49 | 31.61 | 31.78 | 31.47 | 32.14 |
| | SSIM | 0.9455 | 0.9458 | 0.9461 | 0.9474 | 0.9461 | 0.9469 | 0.9476 | 0.9459 | 0.9495 | 0.9162 | 0.9170 | 0.9177 | 0.9197 | 0.9175 | 0.9193 | 0.9208 | 0.9174 | 0.9251 |
| | LPIPS | 0.0889 | 0.0879 | 0.0869 | 0.0833 | 0.0887 | 0.0832 | 0.0835 | 0.0888 | 0.0767 | 0.0984 | 0.0963 | 0.0947 | 0.0916 | 0.0973 | 0.0916 | 0.0890 | 0.097 | 0.0823 |
| | DISTS | 0.0571 | 0.0567 | 0.0567 | 0.0547 | 0.0564 | 0.0555 | 0.0543 | 0.0569 | 0.0514 | 0.0692 | 0.0688 | 0.0682 | 0.0662 | 0.0686 | 0.0667 | 0.0649 | 0.0685 | 0.0612 |
| ×3 | PSNR | 32.34 | 32.38 | 32.43 | 32.51 | 32.48 | 32.52 | 32.61 | 32.42 | 32.89 | 27.88 | 27.93 | 27.99 | 28.09 | 27.98 | 28.07 | 28.12 | 27.97 | 28.46 |
| | SSIM | 0.8877 | 0.8887 | 0.8892 | 0.8902 | 0.8892 | 0.8910 | 0.8911 | 0.8888 | 0.8960 | 0.8292 | 0.8312 | 0.8321 | 0.8345 | 0.8317 | 0.8347 | 0.8353 | 0.8314 | 0.8443 |
| | LPIPS | 0.1977 | 0.1935 | 0.1915 | 0.1903 | 0.1945 | 0.1859 | 0.1873 | 0.1940 | 0.1782 | 0.2200 | 0.2128 | 0.2110 | 0.2075 | 0.2148 | 0.2056 | 0.2043 | 0.2142 | 0.1929 |
| | DISTS | 0.1036 | 0.1035 | 0.1032 | 0.1015 | 0.1031 | 0.1414 | 0.0984 | 0.1041 | 0.0963 | 0.1255 | 0.1250 | 0.1242 | 0.1219 | 0.1246 | 0.1219 | 0.1174 | 0.1256 | 0.1155 |
| ×4 | PSNR | 33.36 | 30.43 | 30.47 | 30.57 | 30.51 | 30.56 | 30.67 | 30.46 | 30.89 | 26.13 | 26.21 | 26.26 | 26.36 | 26.25 | 26.33 | 26.42 | 26.23 | 26.65 |
| | SSIM | 0.8367 | 0.8388 | 0.8395 | 0.8415 | 0.8396 | 0.8416 | 0.8431 | 0.8389 | 0.8486 | 0.7577 | 0.7614 | 0.7627 | 0.7666 | 0.7621 | 0.7656 | 0.7681 | 0.7615 | 0.7774 |
| | LPIPS | 0.2723 | 0.2662 | 0.2647 | 0.2616 | 0.2680 | 0.2607 | 0.2585 | 0.2684 | 0.2518 | 0.3074 | 0.2978 | 0.2957 | 0.2899 | 0.2998 | 0.2921 | 0.2865 | 0.3007 | 0.2777 |
| | DISTS | 0.1394 | 0.1403 | 0.1397 | 0.1384 | 0.1401 | 0.1379 | 0.1370 | 0.1406 | 0.1301 | 0.1666 | 0.1678 | 0.1664 | 0.1647 | 0.1675 | 0.1647 | 0.1631 | 0.1679 | 0.1554 |
| ×6 | PSNR | 28.07 | 28.20 | 28.26 | 28.34 | 28.26 | 28.31 | 28.38 | 28.19 | 28.60 | 24.29 | 24.38 | 24.43 | 24.50 | 24.41 | 24.47 | 24.54 | 24.38 | 24.71 |
| | SSIM | 0.7618 | 0.7669 | 0.7679 | 0.7704 | 0.7674 | 0.7699 | 0.7711 | 0.7648 | 0.7784 | 0.6612 | 0.6684 | 0.6696 | 0.6736 | 0.6685 | 0.6722 | 0.6753 | 0.6654 | 0.6852 |
| | LPIPS | 0.3696 | 0.3594 | 0.3657 | 0.3610 | 0.3646 | 0.3606 | 0.3547 | 0.3728 | 0.3435 | 0.4212 | 0.4080 | 0.4162 | 0.4088 | 0.4124 | 0.4115 | 0.3978 | 0.4226 | 0.3879 |
| | DISTS | 0.1938 | 0.1954 | 0.1954 | 0.1939 | 0.1952 | 0.1934 | 0.1934 | 0.1969 | 0.1835 | 0.2247 | 0.2265 | 0.2256 | 0.2229 | 0.2262 | 0.2236 | 0.2217 | 0.2274 | 0.2120 |
| ×8 | PSNR | 26.72 | 26.87 | 26.93 | 27.00 | 26.91 | 26.97 | 27.04 | 26.76 | 27.22 | 23.23 | 23.32 | 23.37 | 23.43 | 23.34 | 23.40 | 23.47 | 23.27 | 23.58 |
| | SSIM | 0.7135 | 0.7207 | 0.7218 | 0.7243 | 0.7207 | 0.7235 | 0.7256 | 0.7155 | 0.7321 | 0.6032 | 0.6123 | 0.6137 | 0.6171 | 0.6118 | 0.6156 | 0.6194 | 0.6059 | 0.6269 |
| | LPIPS | 0.4365 | 0.4212 | 0.4321 | 0.4261 | 0.4285 | 0.4264 | 0.4169 | 0.4445 | 0.4077 | 0.5020 | 0.4812 | 0.4939 | 0.4848 | 0.4868 | 0.4883 | 0.4703 | 0.5068 | 0.4611 |
| | DISTS | 0.2305 | 0.2337 | 0.2348 | 0.2330 | 0.2341 | 0.2328 | 0.2314 | 0.2386 | 0.2214 | 0.2643 | 0.2673 | 0.2671 | 0.2640 | 0.2677 | 0.2654 | 0.2619 | 0.2713 | 0.2518 |
| ×12 | PSNR | 25.06 | 25.21 | 25.28 | 25.34 | 25.23 | 25.31 | 25.37 | 24.96 | 25.50 | 22.00 | 22.08 | 22.13 | 22.17 | 22.09 | 22.15 | 22.20 | 21.95 | 22.26 |
| | SSIM | 0.6595 | 0.6685 | 0.6693 | 0.6714 | 0.6678 | 0.6706 | 0.6731 | 0.6596 | 0.6777 | 0.5421 | 0.5525 | 0.5533 | 0.5558 | 0.5511 | 0.5542 | 0.5584 | 0.5424 | 0.5632 |
| | LPIPS | 0.5290 | 0.5145 | 0.5300 | 0.5233 | 0.5249 | 0.5246 | 0.5080 | 0.5619 | 0.4975 | 0.6018 | 0.5882 | 0.6047 | 0.5953 | 0.5962 | 0.6013 | 0.5750 | 0.6363 | 0.5642 |
| | DISTS | 0.2852 | 0.2905 | 0.2938 | 0.2914 | 0.2934 | 0.2916 | 0.2885 | 0.3038 | 0.2787 | 0.3210 | 0.3256 | 0.3267 | 0.3238 | 0.3280 | 0.3255 | 0.3203 | 0.3366 | 0.3106 |
| ×16 | PSNR | 24.00 | 24.13 | 24.20 | 24.25 | 24.14 | 24.23 | 24.27 | 23.80 | 24.38 | 21.22 | 21.29 | 21.34 | 21.38 | 21.31 | 21.32 | 21.40 | 21.12 | 21.42 |
| | SSIM | 0.6307 | 0.6402 | 0.6407 | 0.6423 | 0.6394 | 0.6418 | 0.6443 | 0.6306 | 0.6473 | 0.5120 | 0.5221 | 0.5227 | 0.5245 | 0.5209 | 0.5213 | 0.5271 | 0.5122 | 0.5296 |
| | LPIPS | 0.5924 | 0.5754 | 0.5912 | 0.5847 | 0.5876 | 0.5861 | 0.5666 | 0.6325 | 0.5563 | 0.6687 | 0.6529 | 0.6691 | 0.6617 | 0.6622 | 0.6738 | 0.6386 | 0.7101 | 0.6280 |
| | DISTS | 0.3297 | 0.3357 | 0.3398 | 0.3367 | 0.3412 | 0.3371 | 0.3336 | 0.3582 | 0.3242 | 0.3638 | 0.3683 | 0.3701 | 0.3671 | 0.3727 | 0.3687 | 0.3636 | 0.3866 | 0.3538 |
| ×18 | PSNR | 23.57 | 23.71 | 23.77 | 23.83 | 23.71 | 23.81 | 23.85 | 23.37 | 23.93 | 20.92 | 20.99 | 21.04 | 21.07 | 21.00 | 21.03 | 21.09 | 20.81 | 21.11 |
| | SSIM | 0.6212 | 0.6306 | 0.6309 | 0.6323 | 0.6297 | 0.6319 | 0.6344 | 0.6213 | 0.6367 | 0.5027 | 0.5124 | 0.5126 | 0.5142 | 0.5112 | 0.5115 | 0.5165 | 0.503 | 0.5185 |
| | LPIPS | 0.6055 | 0.5966 | 0.6130 | 0.6066 | 0.6083 | 0.6081 | 0.5881 | 0.6563 | 0.5790 | 0.6807 | 0.6749 | 0.6916 | 0.6837 | 0.6828 | 0.6948 | 0.6609 | 0.7343 | 0.6514 |
| | DISTS | 0.3490 | 0.3540 | 0.3584 | 0.3555 | 0.3606 | 0.3557 | 0.3518 | 0.3813 | 0.3419 | 0.3812 | 0.3854 | 0.3875 | 0.3843 | 0.3905 | 0.3852 | 0.3807 | 0.4071 | 0.3710 |
| ×24 | PSNR | 22.63 | 22.74 | 22.81 | 22.84 | 22.74 | 22.83 | 22.87 | 22.41 | 22.90 | 20.25 | 20.31 | 20.35 | 20.39 | 20.32 | 20.34 | 20.40 | 20.11 | 20.38 |
| | SSIM | 0.6027 | 0.6108 | 0.6112 | 0.6119 | 0.6101 | 0.6117 | 0.6141 | 0.6037 | 0.6150 | 0.4854 | 0.4938 | 0.4938 | 0.4845 | 0.4930 | 0.4924 | 0.4967 | 0.4862 | 0.4973 |
| | LPIPS | 0.6512 | 0.6444 | 0.6600 | 0.6539 | 0.6545 | 0.6561 | 0.6352 | 0.7042 | 0.6299 | 0.7234 | 0.7214 | 0.7374 | 0.7292 | 0.7261 | 0.7421 | 0.7067 | 0.7812 | 0.7028 |
| | DISTS | 0.4022 | 0.4009 | 0.4063 | 0.4026 | 0.4106 | 0.4036 | 0.3980 | 0.4380 | 0.3877 | 0.4292 | 0.4274 | 0.4308 | 0.4269 | 0.4348 | 0.4297 | 0.4222 | 0.4579 | 0.4117 |
| ×30 | PSNR | 21.97 | 22.07 | 22.12 | 22.16 | 22.07 | 22.03 | 22.18 | 21.75 | 22.19 | 19.75 | 19.80 | 19.84 | 19.86 | 19.81 | 19.83 | 19.87 | 19.60 | 19.82 |
| | SSIM | 0.5982 | 0.5998 | 0.6000 | 0.6003 | 0.5994 | 0.5966 | 0.6021 | 0.5943 | 0.6025 | 0.4754 | 0.4824 | 0.4823 | 0.4824 | 0.4817 | 0.4818 | 0.4839 | 0.4766 | 0.4842 |
| | LPIPS | 0.7018 | 0.6773 | 0.6914 | 0.6862 | 0.6859 | 0.7137 | 0.6682 | 0.7317 | 0.6648 | 0.7386 | 0.7537 | 0.7676 | 0.7610 | 0.7575 | 0.7645 | 0.7284 | 0.8084 | 0.7368 |
| | DISTS | 0.4474 | 0.4375 | 0.4445 | 0.4400 | 0.4500 | 0.4476 | 0.4339 | 0.4821 | 0.4232 | 0.4702 | 0.4603 | 0.4645 | 0.4597 | 0.4702 | 0.4608 | 0.4535 | 0.4986 | 0.4417 |

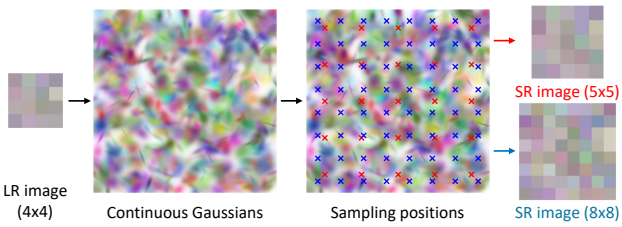


Figure 3. Demonstration of the sampling process in 2D rasterization. A larger upsampling scale factor employs smaller sampling intervals from continuous Gaussians.

**Condition Injection Block.** As shown in Figure 2, we utilize cross-attention to incorporate feature $\mathbf{F}$ into Gaussian embeddings $\mathbf{E}$. Such a technique is widely used in models like Stable Diffusion [52]. To reduce the computational complexity, we perform window-based cross-attention [42] only in pre-defined local windows as follows:

$$\text{Attention}(Q, K, V) = \text{SoftMax}\left(\frac{QK^{\top}}{\sqrt{d}} + B\right)V, \quad (5)$$

where $Q$ is from Gaussian embedding $\mathbf{E}$, $K$ and $V$ are from image feature $\mathbf{F}$. The $i$-th embedding $\mathbf{E}_i$ at position $p_i$ interacts with the $j$-th pixel features within the window. $B$ is the relative position bias in the feature map.

**Gaussian Interaction Block.** In the condition injection block, each Gaussian embedding $\mathbf{E}_i$ is processed independently, resulting in a lack of information exchange among different Gaussian embeddings. To address this issue, we stack $L$ Gaussian interaction blocks to enhance the interaction among Gaussian embeddings. The Gaussian interaction block is designed based on Swin-transformer architecture, which iteratively stacks the window attention layers and shifted window attention layers. In attention layers, we perform self-attention for embeddings whose reference positions are located in the same window, similar to the condition injection block. Besides, we introduce a cross-attention layer to make embeddings scale-aware so that the Gaussian embeddings can learn to adjust the properties according to the given scale factor.

Table 2. Quantitative comparison between representative ASR models and our GSASR. All models use the same RDN [80] backbone as the feature extraction encoder. We test on DIV2K and LSDIR [36] datasets [55] with scaling factors ×2, ×3, ×4, ×6, ×8, ×12, ×16, ×18, ×24, ×30. The best results are highlighted in red. The PSNR and SSIM indices are computed in the Y channel of Ycbcr space.

| Scale | Metrics | Backbone: RDN | | | | | | | | | | | | | | | | | |
|---|---|---|---|---|---|---|---|---|---|---|---|---|---|---|---|---|---|---|---|
| | | Testing Dataset: DIV2K | | | | | | | | | Testing Dataset: LSDIR | | | | | | | | |
| | | Meta -SR | LIIF | LTE | SRNO | LINF | LMF | Ciao -SR | Gaussian -SR | GSASR | Meta -SR | LIIF | LTE | SRNO | LINF | LMF | Ciao -SR | Gaussian -SR | GSASR |
| ×2 | PSNR | 36.54 | 36.37 | 36.41 | 36.53 | 36.53 | 36.48 | 36.67 | 36.54 | 36.73 | 31.97 | 31.87 | 31.96 | 32.10 | 31.94 | 32.02 | 32.16 | 31.95 | 32.26 |
| | SSIM | 0.9483 | 0.9481 | 0.9484 | 0.9493 | 0.9483 | 0.9487 | 0.9494 | 0.9484 | 0.9500 | 0.9224 | 0.9221 | 0.9228 | 0.9247 | 0.9223 | 0.9234 | 0.9247 | 0.9228 | 0.9261 |
| | LPIPS | 0.0816 | 0.0828 | 0.0816 | 0.0783 | 0.0821 | 0.0806 | 0.0797 | 0.0829 | 0.0757 | 0.0872 | 0.0876 | 0.0861 | 0.0832 | 0.0874 | 0.0866 | 0.0839 | 0.0875 | 0.0812 |
| | DISTS | 0.0542 | 0.0543 | 0.0535 | 0.0528 | 0.0541 | 0.0540 | 0.0524 | 0.0543 | 0.0509 | 0.0644 | 0.0645 | 0.0635 | 0.0623 | 0.0645 | 0.0639 | 0.0615 | 0.0640 | 0.0603 |
| ×3 | PSNR | 32.79 | 32.68 | 32.73 | 32.83 | 32.77 | 32.78 | 32.89 | 32.74 | 32.97 | 28.34 | 28.26 | 28.34 | 28.45 | 28.30 | 28.37 | 28.46 | 28.33 | 28.56 |
| | SSIM | 0.8935 | 0.8934 | 0.8938 | 0.8951 | 0.8936 | 0.8947 | 0.8952 | 0.8939 | 0.8970 | 0.8399 | 0.8398 | 0.8409 | 0.8435 | 0.8398 | 0.8421 | 0.8432 | 0.8407 | 0.8462 |
| | LPIPS | 0.1850 | 0.1842 | 0.1837 | 0.1817 | 0.1846 | 0.1807 | 0.1821 | 0.1847 | 0.1768 | 0.1997 | 0.1983 | 0.1979 | 0.1947 | 0.1995 | 0.1954 | 0.1953 | 0.1993 | 0.1908 |
| | DISTS | 0.1000 | 0.0998 | 0.0987 | 0.0980 | 0.0999 | 0.0984 | 0.0965 | 0.0998 | 0.0955 | 0.1192 | 0.1188 | 0.1176 | 0.1159 | 0.1194 | 0.1169 | 0.1139 | 0.1189 | 0.1139 |
| ×4 | PSNR | 30.78 | 30.71 | 30.75 | 30.85 | 30.77 | 30.81 | 30.91 | 30.76 | 30.96 | 26.53 | 26.48 | 26.54 | 26.64 | 26.51 | 26.58 | 26.66 | 26.53 | 26.73 |
| | SSIM | 0.8455 | 0.8449 | 0.8459 | 0.8478 | 0.8453 | 0.8467 | 0.8481 | 0.8457 | 0.8500 | 0.7724 | 0.7714 | 0.7734 | 0.7767 | 0.7719 | 0.7744 | 0.7770 | 0.7727 | 0.7801 |
| | LPIPS | 0.2568 | 0.2566 | 0.2558 | 0.2525 | 0.2574 | 0.2546 | 0.2525 | 0.2570 | 0.2505 | 0.2831 | 0.2838 | 0.2822 | 0.2771 | 0.2840 | 0.2817 | 0.2768 | 0.2837 | 0.2752 |
| | DISTS | 0.1341 | 0.1354 | 0.1341 | 0.1330 | 0.1355 | 0.1341 | 0.1327 | 0.1347 | 0.1288 | 0.1581 | 0.1603 | 0.1589 | 0.1567 | 0.1609 | 0.1584 | 0.1563 | 0.1595 | 0.1533 |
| ×6 | PSNR | 28.40 | 28.44 | 28.49 | 28.57 | 28.48 | 28.52 | 28.61 | 28.46 | 28.65 | 24.55 | 24.59 | 24.64 | 24.70 | 24.61 | 24.66 | 24.73 | 24.60 | 24.77 |
| | SSIM | 0.7715 | 0.7739 | 0.7749 | 0.7772 | 0.7739 | 0.7757 | 0.7777 | 0.7727 | 0.7800 | 0.6756 | 0.6791 | 0.6806 | 0.6841 | 0.6787 | 0.6815 | 0.6853 | 0.6772 | 0.6881 |
| | LPIPS | 0.3505 | 0.3468 | 0.3551 | 0.3510 | 0.3523 | 0.3534 | 0.3452 | 0.3584 | 0.3443 | 0.3960 | 0.3915 | 0.4020 | 0.3964 | 0.3961 | 0.4009 | 0.3864 | 0.4043 | 0.3867 |
| | DISTS | 0.1837 | 0.1882 | 0.1878 | 0.1861 | 0.1890 | 0.1873 | 0.1867 | 0.1880 | 0.1817 | 0.2110 | 0.2166 | 0.2161 | 0.2131 | 0.2181 | 0.2154 | 0.2131 | 0.2167 | 0.2093 |
| ×8 | PSNR | 26.97 | 27.07 | 27.13 | 27.20 | 27.11 | 27.16 | 27.24 | 26.99 | 27.28 | 23.44 | 23.49 | 23.54 | 23.60 | 23.52 | 23.57 | 23.63 | 23.45 | 23.63 |
| | SSIM | 0.7222 | 0.7274 | 0.7286 | 0.7308 | 0.7272 | 0.7293 | 0.7317 | 0.7228 | 0.7339 | 0.6151 | 0.6221 | 0.6230 | 0.6264 | 0.6211 | 0.6240 | 0.6281 | 0.6156 | 0.6299 |
| | LPIPS | 0.4133 | 0.4072 | 0.4214 | 0.4166 | 0.4163 | 0.4188 | 0.4075 | 0.4290 | 0.4060 | 0.4679 | 0.4627 | 0.4798 | 0.4729 | 0.4711 | 0.4772 | 0.4592 | 0.4875 | 0.4593 |
| | DISTS | 0.2181 | 0.2251 | 0.2268 | 0.2248 | 0.2273 | 0.2260 | 0.2244 | 0.2285 | 0.2192 | 0.2489 | 0.2562 | 0.2569 | 0.2537 | 0.2588 | 0.2563 | 0.2528 | 0.2601 | 0.2490 |
| ×12 | PSNR | 25.23 | 25.39 | 25.45 | 25.52 | 25.41 | 25.48 | 25.55 | 25.12 | 25.56 | 22.13 | 22.21 | 22.26 | 22.31 | 22.22 | 22.28 | 22.33 | 22.06 | 22.30 |
| | SSIM | 0.6653 | 0.6739 | 0.6748 | 0.6768 | 0.6730 | 0.6754 | 0.6783 | 0.6648 | 0.6794 | 0.5494 | 0.5597 | 0.5605 | 0.5629 | 0.5576 | 0.5608 | 0.5651 | 0.5484 | 0.5656 |
| | LPIPS | 0.5001 | 0.4981 | 0.5180 | 0.5132 | 0.5120 | 0.5153 | 0.4982 | 0.5455 | 0.4947 | 0.5671 | 0.5685 | 0.5899 | 0.5823 | 0.5803 | 0.5884 | 0.5635 | 0.6174 | 0.5621 |
| | DISTS | 0.2703 | 0.2809 | 0.2857 | 0.2835 | 0.2855 | 0.2844 | 0.2811 | 0.2921 | 0.2759 | 0.3055 | 0.3138 | 0.3165 | 0.3133 | 0.3187 | 0.3160 | 0.3116 | 0.3252 | 0.3077 |
| ×16 | PSNR | 24.12 | 24.30 | 24.36 | 24.42 | 24.30 | 24.38 | 24.44 | 23.93 | 24.44 | 19.34 | 21.40 | 21.45 | 21.49 | 21.41 | 21.45 | 21.50 | 21.20 | 21.47 |
| | SSIM | 0.6346 | 0.6446 | 0.6452 | 0.6467 | 0.6433 | 0.6456 | 0.6484 | 0.6340 | 0.6487 | 0.4813 | 0.5273 | 0.5277 | 0.5294 | 0.5253 | 0.5269 | 0.5318 | 0.5156 | 0.5318 |
| | LPIPS | 0.5606 | 0.5580 | 0.5788 | 0.5739 | 0.5751 | 0.5760 | 0.5572 | 0.6166 | 0.5537 | 0.6762 | 0.6343 | 0.6556 | 0.6487 | 0.6488 | 0.6598 | 0.6281 | 0.6932 | 0.6261 |
| | DISTS | 0.3117 | 0.3243 | 0.3312 | 0.3288 | 0.3324 | 0.3295 | 0.3268 | 0.3455 | 0.3211 | 0.3845 | 0.3566 | 0.3605 | 0.3575 | 0.3638 | 0.3596 | 0.3562 | 0.3745 | 0.3512 |
| ×18 | PSNR | 23.69 | 23.87 | 23.93 | 23.99 | 23.87 | 23.96 | 24.01 | 23.48 | 23.98 | 20.99 | 21.09 | 21.14 | 21.17 | 21.10 | 21.13 | 21.18 | 20.88 | 21.14 |
| | SSIM | 0.6244 | 0.6346 | 0.6349 | 0.6362 | 0.6333 | 0.6353 | 0.6380 | 0.6239 | 0.6379 | 0.5056 | 0.5165 | 0.5168 | 0.5181 | 0.5147 | 0.5160 | 0.5205 | 0.5056 | 0.5203 |
| | LPIPS | 0.5776 | 0.5805 | 0.6013 | 0.5968 | 0.5957 | 0.5987 | 0.5796 | 0.6418 | 0.5766 | 0.6489 | 0.6575 | 0.6490 | 0.6720 | 0.6696 | 0.6822 | 0.6511 | 0.7188 | 0.6497 |
| | DISTS | 0.3303 | 0.3419 | 0.3499 | 0.3476 | 0.3513 | 0.3480 | 0.3455 | 0.3676 | 0.3391 | 0.3633 | 0.3733 | 0.3784 | 0.3752 | 0.3814 | 0.3764 | 0.3740 | 0.3944 | 0.3682 |
| ×24 | PSNR | 22.71 | 22.87 | 22.92 | 22.97 | 22.87 | 22.93 | 22.99 | 22.49 | 22.96 | 19.26 | 20.39 | 20.44 | 20.47 | 20.41 | 20.43 | 20.48 | 20.16 | 20.42 |
| | SSIM | 0.6041 | 0.6139 | 0.6138 | 0.6145 | 0.6128 | 0.6136 | 0.6166 | 0.6048 | 0.6162 | 0.4728 | 0.4967 | 0.4965 | 0.4973 | 0.4953 | 0.4955 | 0.4995 | 0.4873 | 0.4985 |
| | LPIPS | 0.6273 | 0.6301 | 0.6505 | 0.6461 | 0.6423 | 0.6487 | 0.6292 | 0.6939 | 0.6275 | 0.7112 | 0.7073 | 0.7274 | 0.7207 | 0.7143 | 0.7316 | 0.7005 | 0.7701 | 0.7006 |
| | DISTS | 0.3830 | 0.3865 | 0.3978 | 0.3955 | 0.4008 | 0.3961 | 0.3932 | 0.4224 | 0.3851 | 0.4205 | 0.4145 | 0.4220 | 0.4185 | 0.4260 | 0.4212 | 0.4172 | 0.4434 | 0.4095 |
| ×30 | PSNR | 17.25 | 22.18 | 22.23 | 22.27 | 32.18 | 22.18 | 22.28 | 21.81 | 22.23 | 19.78 | 19.86 | 19.91 | 19.93 | 19.89 | 19.90 | 19.94 | 19.64 | 19.86 |
| | SSIM | 0.5546 | 0.6016 | 0.6017 | 0.6024 | 0.6010 | 0.5995 | 0.6041 | 0.5947 | 0.6032 | 0.4758 | 0.4842 | 0.4840 | 0.4844 | 0.4835 | 0.4837 | 0.4861 | 0.4770 | 0.4851 |
| | LPIPS | 0.6817 | 0.6652 | 0.6833 | 0.6799 | 0.6757 | 0.7009 | 0.6627 | 0.7247 | 0.6633 | 0.7164 | 0.7418 | 0.7598 | 0.7540 | 0.7468 | 0.7570 | 0.7269 | 0.8009 | 0.7358 |
| | DISTS | 0.4405 | 0.4215 | 0.4359 | 0.4332 | 0.4394 | 0.4361 | 0.4301 | 0.4650 | 0.4213 | 0.4509 | 0.4454 | 0.4562 | 0.4520 | 0.4605 | 0.4536 | 0.4495 | 0.4823 | 0.4407 |

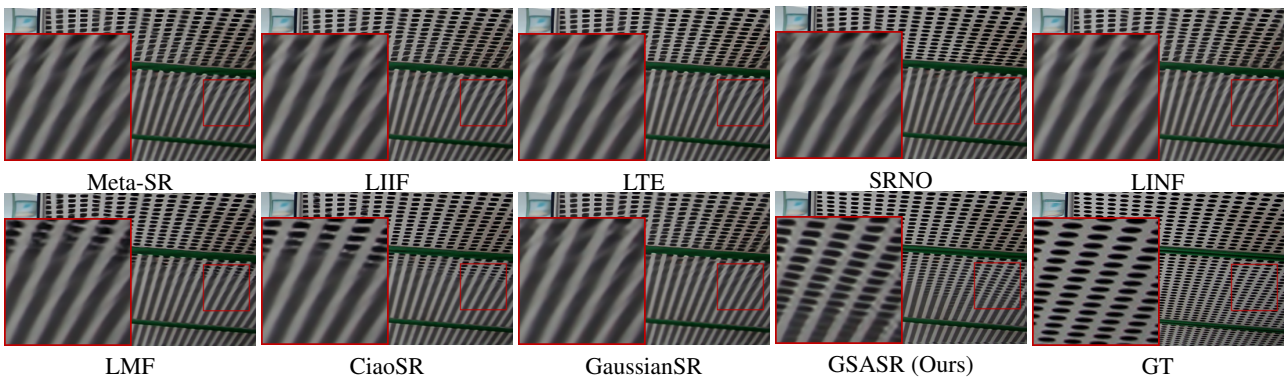


Figure 4. Visualization of GSASR and the competing methods under ×4 scaling factor with EDSR [40] feature extraction backbone. The competing methods result in blurry details, while GSASR generates much clear textures.

**Gaussian Primary Head.** We employ several disentangled property heads to convert Gaussian embeddings $\mathbf{E}$ into 2D Gaussians $\mathcal{G}$. The $i$-th Gaussian embedding $\mathbf{E}_i$ is fed into a lightweight MLP to output its opacity $\alpha_i$, color $c_i$, stand deviation $\sigma_i$, reference offset $o_i$, and correlation $\rho_i$. Note that the position is obtained by adding the reference position and predicted offset $\mu_i = p_i + o_i$. The five property heads are decoupled so that different heads can be adapted to predict

specific properties. We apply the tanh function to ensure $\rho \in [-1, 1]$, and use the sigmoid function for $\{\alpha, c, \sigma\}$ to ensure that their values are physically meaningful. No activation function is applied to $o$ since the positions of Gaussians in 2D images are expected to be free.

**Rendering.** In Eq. 4, the rasterization determines the sampling interval of the 2D Gaussians based on the scale factor. As illustrated in Figure 3, larger upsampling factors use smaller sampling intervals, while the smaller upsampling factors use larger intervals. Due to the excellent representational capacity of Gaussians, high-quality sampling results can be achieved even in areas with complex textures. After rendering the SR image from rasterization, it is compared with the HR ground truth to calculate the loss $L_1$.

# 4. Experiments

## 4.1. Experimental Setup

**Training Details**. We utilize the widely-used DIV2K [55] dataset as training set. We follow [2, 10] to fix LR patches to $48 \times 48$. The scaling factor $s$ is randomly selected from $[1.0, 4.0]$. We firstly crop $48s \times 48s$ GT patch from the original full-size GT image, and then apply the bicubic downsampling [2] to obtain the corresponding LR patches. We employ EDSR [40] and RDN [80] as the image encoder backbones to extract feature from the input LR images. We train our GSARS on 4 NVIDIA A100 GPUs for $500,000$ iterations, with a batch size of 64. The initial learning rate is set to $2e^{-4}$, and halves at $250,000$, $400,000$, $450,000$, $475,000$ iterations. The Adam [29] optimizer is utilized. To speed up the convergence of the training progress, we set the number of warm-up iterations to $2,000$.

**Comparison Methods**. We compare our proposed GSASR with Meta-SR [24], LIIF [10], LTE [32], SRNO [64], LINF [69], CiaoSR [2], LMF [22], and GaussianSR [23].

**Evaluation Protocols**. We evaluate the competing models on Set5 [1], Set14 [72], DIV2K100 [55], Urban100 [25], BSDS100 [45], Manga109 [46], General100 [16], and LSDIR [36] datasets under scaling factors $\times 2$, $\times 3$, $\times 4$, $\times 6$, $\times 8$, $\times 12$. To validate the generalization on higher scaling factors, we further report the results with $\times 16$, $\times 18$, $\times 24$, $\times 30$ scaling factors on DIV2K100 [55] and LSDIR [36] datasets. For performance measurement, we report PSNR, SSIM [63], LPIPS [75], and DISTS [14] indices. The PSNR and SSIM are computed in the Y channel of Ycbcr space. For the comparison of computational cost, we crop 100 GT patches with $720 \times 720$ resolution from DIV2K [55], and use bicubic interpolation to generate the corresponding LR images with scaling factors $\times 2$, $\times 3$, $\times 4$, $\times 6$, $\times 8$, $\times 12$. We report the average inference time (ms) and GPU memory usage (MB) on a single NVIDIA A100 GPU.

## 4.2. Experiment Results

**Quantitative Results**. Table 1 and Table 2 show the numerical results of our proposed GSASR and other comparison methods. One could see that GSASR outperforms existing methods in terms of both fidelity metrics (PSNR and SSIM [63]) and perceptual quality metrics (LPIPS [75] and DISTS [14]) under both the EDSR [40] and RDN [80] backbones and scaling factors from $\times 2$ to $\times 30$. It obtains significant improvements over the methods based on INR, exhibiting greater potential for ASR. Compared with the recent GaussianSR method [23], which also employs GS for feature representation, GSASR shows clear advantages. GSASR predicts the position of Gaussians via an end-to-end manner, while GaussianSR [23] simply replaces the position parameters with the fixed position of RGB pixels of the LR image and loses representation capability. Besides, GaussianSR lacks GPU/CUDA-based rasterization to accelerate the inference speed and it fixes the number of Gaussians to 100, no matter how large the scaling factor is. Therefore, the performance of GaussianSR drops a lot under high magnification factors. On the contrary, we present an efficient 2D GPU/CUDA-based rasterization to embed much more Gaussians to promote ASR performance. As a result, although GSASR is trained with a scaling factor from 1.0 to 4.0, it could not only obtain excellent performance for in-distribution scaling factors (*i.e.*, scaling factor is less than 4), but also show strong capability in dealing with out-of-distribution situations (*i.e.*, the scaling factor is larger than 4). More results on Set5 [1], Set14 [72], Urban100 [25], BSDS100 [45], Manga109 [46], General100 [16] could be found in the **Appendix**.

**Qualitative Results**. Figure 4 and Figure 5 show the qualitative comparison of competing methods. We can see that the compared methods mostly produce blurry details, for example, the holes in Figure 4, while GSASR generates much clearer edges and details, owing to the strong representation ability from 2D Gaussians. More visualization results can be found in the **Appendix**. To explain why GSASR works well for the ASR task, we visualize the positions together with the shape of Gaussians in Figure 6. One could see that the positions of Gaussians tend to cluster in areas with complex textures (such as the windows), while they are uniformly distributed in flat areas (such as the sky). This validates that our proposed strategy is highly suitable for restoring complex texture details. Meanwhile, from the blue box and green box in Figure 6, one could find that the Gaussians will adaptively adjust their orientations and scales based on the direction and shape of the textures.

**Computational Costs**. Table 3 shows that GSASR surpasses all the competing methods in most of the fidelity (PSNR, SSIM) and perceptual (LPIPS, DISTS) measures. In terms of speed, GSASR is nearly twice as fast as the state-of-the-art method CiaoSR [2] under $\times 3, \times 4$ scaling

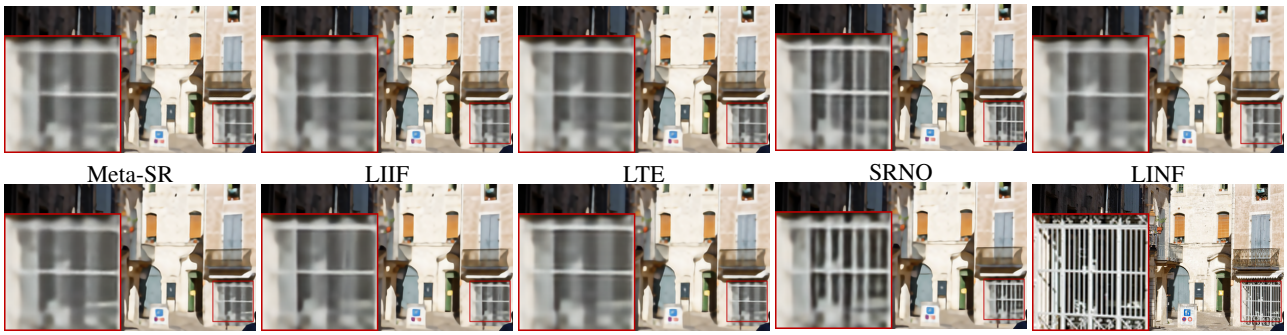


Figure 5. Visualization of GSASR and the competing methods under $\times 6$ scaling factor with RDN [80] feature extraction backbone. The competing methods produce blurry textures, while GSASR generates much clearer contents.

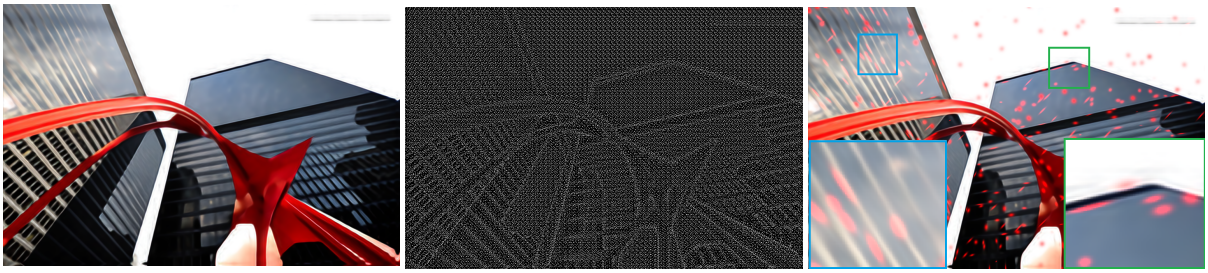


Figure 6. Demonstration of the rich expressiveness of Gaussians for ASR. The position distribution is obtained by setting $\{\sigma, \rho, c\}$ to fixed values. In the middle image, one could observe that Gaussians are evenly distributed in regions with simple textures or flatten area (such as the sky), while their positions are adjusted in regions with complex textures to fit details. (**Please zoom in for better observation**.) In the right image, we randomly select parts of Gaussians and highlight their colors to red. One can see that 2D Gaussians can learn to fit the different object shapes ($e.g.$, the edge of window).

factors, and speed advantage becomes more significant when handling with larger scaling factors. Thanks to the efficient 2D GPU/CUDA-based rasterization, GSASR could render an image with high speed without sacrificing the reconstruction fidelity. The computational cost with RDN backbone could be found in the **Appendix**.

**Ablation Study**. We conduct ablation studies on the number of Gaussians $N$, and the functionality of the reference position. Details are in the **Appendix**.

## 5. Conclusion and Limitation

We presented GSASR, a brandly-new 2D GS-based ASR model. To adapt GS to the ASR task, we firstly elaborately designed an architecture to covert an LR input to image-conditioned Gaussians, then implemented an efficient differentiable scale-aware 2D GPU/CUDA-based rasterization to render images with both high quality and fast speed. Through sampling values from Gaussians, we could render an output image with arbitrary magnification factors. Extensive experiments demonstrated that our GSASR model has a much more powerful representation capability, together with more friendly computational costs, than Implicit Neural Function based methods.

**Limitations**. GSASR still has some limitations. First, its performance depends on the number of Gaussians, especially under ultra-high scaling factors. While more Gaussians could bring better performance, it will sacrifice the inference speed. Second, to convert an image into Gaussians, a large number of parameters are used to fit the complex mapping function. How to reduce the number of parameters needs further investigation.

## References

[1] Marco Bevilacqua, Aline Roumy, Christine Guillemot, and Marie Line Alberi-Morel. Low-complexity single-image super-resolution based on nonnegative neighbor embedding. In *BMVC*, pages 135.1–135.10, 2012. 7

[2] Jiezhang Cao, Qin Wang, Yongqin Xian, Yawei Li, Bingbing Ni, Zhiming Pi, Kai Zhang, Yulun Zhang, Radu Timofte, and Luc Van Gool. Ciaosr: Continuous implicit attention-in-attention network for arbitrary-scale image super-resolution. In *Proceedings of the IEEE/CVF Conference on Computer Vision and Pattern Recognition*, pages 1796–1807, 2023. 2, 3, 7

[3] Nicolas Carion, Francisco Massa, Gabriel Synnaeve, Nicolas

Table 3. Comparison of computational costs. We report the results using EDSR-backbone [40] as image encoder. Apart from the PSNR/SSIM/LPIPS/DISTS metrics, we report the average inference time (ms) and the GPU memory usage (MB). The best results are highlighted in red.

| Scale | Computational Cost and Performance | Backbone: EDSR<br>Testing GT Size: 720 * 720 | | | | | | | | |
|---|---|---|---|---|---|---|---|---|---|---|
| | | Meta-SR | LIIF | LTE | SRNO | LINF | LMF | CiaoSR | GaussianSR | GSASR |
| ×2 | PSNR | 37.09 | 37.14 | 37.16 | 37.34 | 37.42 | 37.29 | 37.59 | 37.18 | 37.84 |
| | SSIM | 0.9475 | 0.9487 | 0.9491 | 0.9501 | 0.9490 | 0.9498 | 0.9502 | 0.9489 | 0.9522 |
| | LPIPS | 0.0787 | 0.0777 | 0.0768 | 0.0743 | 0.0785 | 0.0736 | 0.0744 | 0.0785 | 0.0676 |
| | DISTS | 0.0741 | 0.0737 | 0.0736 | 0.0713 | 0.0731 | 0.0724 | 0.0710 | 0.0738 | 0.0676 |
| | Inference Time | 186 | 454 | 126 | 107 | 86 | 209 | 2372 | 754 | 1573 |
| | GPU Memory | 670 | 548 | 490 | 6301 | 3573 | 4005 | 49152 | 5200 | 13367 |
| ×3 | PSNR | 33.39 | 33.44 | 33.45 | 33.59 | 33.63 | 33.56 | 33.76 | 33.47 | 34.04 |
| | SSIM | 0.8921 | 0.8931 | 0.8935 | 0.8953 | 0.8936 | 0.8953 | 0.8955 | 0.8932 | 0.9004 |
| | LPIPS | 0.1813 | 0.1778 | 0.1756 | 0.1729 | 0.1783 | 0.1701 | 0.1718 | 0.1780 | 0.1625 |
| | DISTS | 0.1258 | 0.1257 | 0.1255 | 0.1230 | 0.1255 | 0.1236 | 0.1201 | 0.1262 | 0.1182 |
| | Inference Time | 161 | 438 | 118 | 114 | 89 | 147 | 2016 | 717 | 806 |
| | GPU Memory | 493 | 570 | 333 | 6282 | 3412 | 1798 | 10002 | 5138 | 6000 |
| ×4 | PSNR | 31.38 | 31.48 | 31.48 | 31.65 | 31.62 | 31.60 | 31.79 | 31.49 | 32.01 |
| | SSIM | 0.8417 | 0.8437 | 0.8444 | 0.8472 | 0.8444 | 0.8466 | 0.8482 | 0.8437 | 0.8536 |
| | LPIPS | 0.2545 | 0.2490 | 0.2472 | 0.2429 | 0.2506 | 0.2438 | 0.2416 | 0.2511 | 0.2344 |
| | DISTS | 0.1638 | 0.1652 | 0.1646 | 0.1626 | 0.1653 | 0.1930 | 0.1617 | 0.1656 | 0.1542 |
| | Inference Time | 47 | 182 | 114 | 95 | 66 | 68 | 1165 | 686 | 543 |
| | GPU Memory | 432 | 308 | 279 | 6275 | 3357 | 1139 | 3331 | 5048 | 3420 |
| ×6 | PSNR | 29.08 | 29.24 | 29.25 | 29.39 | 29.33 | 29.34 | 29.51 | 29.19 | 29.69 |
| | SSIM | 0.7686 | 0.7735 | 0.7744 | 0.7777 | 0.7738 | 0.7766 | 0.7790 | 0.7715 | 0.7851 |
| | LPIPS | 0.3455 | 0.3362 | 0.3420 | 0.3361 | 0.3411 | 0.3374 | 0.3298 | 0.3492 | 0.3223 |
| | DISTS | 0.2179 | 0.2199 | 0.2195 | 0.2176 | 0.2201 | 0.2179 | 0.2171 | 0.2214 | 0.2083 |
| | Inference Time | 46 | 176 | 118 | 94 | 65 | 55 | 731 | 692 | 265 |
| | GPU Memory | 387 | 264 | 239 | 6270 | 3316 | 912 | 1548 | 5224 | 1578 |
| ×8 | PSNR | 27.74 | 27.89 | 27.94 | 28.04 | 27.97 | 28.00 | 28.14 | 27.77 | 28.25 |
| | SSIM | 0.7216 | 0.7284 | 0.7297 | 0.7326 | 0.7285 | 0.7314 | 0.7345 | 0.7235 | 0.7397 |
| | LPIPS | 0.4132 | 0.3956 | 0.4062 | 0.3988 | 0.4025 | 0.4017 | 0.3892 | 0.4187 | 0.3810 |
| | DISTS | 0.2543 | 0.2569 | 0.2573 | 0.2555 | 0.2576 | 0.2570 | 0.2542 | 0.2623 | 0.2448 |
| | Inference Time | 42 | 170 | 112 | 96 | 64 | 64 | 621 | 666 | 195 |
| | GPU Memory | 371 | 248 | 224 | 6269 | 3302 | 832 | 1503 | 5012 | 1051 |
| ×12 | PSNR | 26.03 | 26.18 | 26.23 | 26.32 | 26.24 | 26.28 | 26.39 | 25.91 | 26.50 |
| | SSIM | 0.6687 | 0.6773 | 0.6783 | 0.6805 | 0.6768 | 0.6796 | 0.6825 | 0.6688 | 0.6864 |
| | LPIPS | 0.4990 | 0.4861 | 0.5011 | 0.4941 | 0.4958 | 0.4959 | 0.4769 | 0.5314 | 0.4701 |
| | DISTS | 0.3063 | 0.3114 | 0.3141 | 0.3113 | 0.3140 | 0.3127 | 0.3084 | 0.3241 | 0.3007 |
| | Inference Time | 41 | 172 | 113 | 91 | 64 | 52 | 540 | 688 | 91 |
| | GPU Memory | 360 | 237 | 214 | 6268 | 3292 | 775 | 1470 | 5214 | 472 |


Usunier, Alexander Kirillov, and Sergey Zagoruyko. End-to-end object detection with transformers. In *European Conference on Computer Vision*, pages 213–229, 2020. 2

[4] David Charatan, Sizhe Lester Li, Andrea Tagliasacchi, and Vincent Sitzmann. pixelsplat: 3d gaussian splats from image pairs for scalable generalizable 3d reconstruction. In *Proceedings of the IEEE/CVF Conference on Computer Vision and Pattern Recognition*, pages 19457–19467, 2024. 2

[5] Du Chen, Jie Liang, Xindong Zhang, Ming Liu, Hui Zeng, and Lei Zhang. Human guided ground-truth generation for realistic image super-resolution. In *IEEE Conference on Computer Vision and Pattern Recognition*, pages 14082–14091. IEEE, 2023. 1, 2

[6] Du Chen, Zhengqiang Zhang, Jie Liang, and Lei Zhang. Ssl: A self-similarity loss for improving generative image super-resolution. In *Proceedings of the 32nd ACM International Conference on Multimedia*, pages 3189–3198, 2024. 1

[7] Hao-Wei Chen, Yu-Syuan Xu, Min-Fong Hong, Yi-Min Tsai, Hsien-Kai Kuo, and Chun-Yi Lee. Cascaded local implicit transformer for arbitrary-scale super-resolution. In *IEEE Conference on Computer Vision and Pattern Recognition*, pages 18257–18267. IEEE, 2023. 3

[8] Wenbo Chen and Ligang Liu. Deblur-gs: 3d gaussian splatting from camera motion blurred images. *Proceedings of the ACM on Computer Graphics and Interactive Techniques*, 7 (1):1–15, 2024. 2

[9] Xiangyu Chen, Xintao Wang, Jiantao Zhou, Yu Qiao, and Chao Dong. Activating more pixels in image super-

resolution transformer. In *IEEE Conference on Computer Vision and Pattern Recognition*, pages 22367–22377. IEEE, 2023. 1, 2

[10] Yinbo Chen, Sifei Liu, and Xiaolong Wang. Learning continuous image representation with local implicit image function. In *IEEE Conference on Computer Vision and Pattern Recognition*, pages 8628–8638, 2021. 1, 2, 3, 7

[11] Yiwen Chen, Zilong Chen, Chi Zhang, Feng Wang, Xiaofeng Yang, Yikai Wang, Zhongang Cai, Lei Yang, Huaping Liu, and Guosheng Lin. Gaussianeditor: Swift and controllable 3d editing with gaussian splatting. In *IEEE/CVF Conference on Computer Vision and Pattern Recognition*, pages 21476–21485, 2024. 2

[12] Zilong Chen, Feng Wang, Yikai Wang, and Huaping Liu. Text-to-3d using gaussian splatting. In *IEEE/CVF Conference on Computer Vision and Pattern Recognition*, pages 21401–21412, 2024. 2

[13] Haram Choi, Jeongmin Lee, and Jihoon Yang. N-gram in swin transformers for efficient lightweight image super-resolution. In *IEEE Conference on Computer Vision and Pattern Recognition*, pages 2071–2081. IEEE, 2023. 2

[14] Keyan Ding, Kede Ma, Shiqi Wang, and Eero P Simoncelli. Image quality assessment: Unifying structure and texture similarity. *IEEE Transactions on Pattern Analysis and Machine Intelligence*, 44(5):2567–2581, 2020. 7

[15] Chao Dong, Chen Change Loy, Kaiming He, and Xiaoou Tang. Learning a deep convolutional network for image super-resolution. In *European Conference on Computer Vision*, pages 184–199. Springer, 2014. 2

[16] Chao Dong, Chen Change Loy, and Xiaoou Tang. Accelerating the super-resolution convolutional neural network. In *European Conference on Computer Vision*, pages 391–407. Springer, 2016. 1, 2, 7

[17] Garas Gendy, Nabil Sabor, Jingchao Hou, and Guanghui He. A simple transformer-style network for lightweight image super-resolution. In *IEEE Conference on Computer Vision and Pattern Recognition*, pages 1484–1494, 2023. 2

[18] Sharath Girish, Kamal Gupta, and Abhinav Shrivastava. Eagles: Efficient accelerated 3d gaussians with lightweight encodings. In *European Conference on Computer Vision*, 2024. 2

[19] Antoine Guédon and Vincent Lepetit. Sugar: Surface-aligned gaussian splatting for efficient 3d mesh reconstruction and high-quality mesh rendering. In *IEEE/CVF Conference on Computer Vision and Pattern Recognition*, pages 5354–5363, 2024. 2

[20] Gaurav Gupta, Xiongye Xiao, and Paul Bogdan. Multiwavelet-based operator learning for differential equations. *Advances in Neural Information Processing Systems*, 34:24048–24062, 2021. 3

[21] Xiangyu He, Zitao Mo, Peisong Wang, Yang Liu, Mingyuan Yang, and Jian Cheng. Ode-inspired network design for single image super-resolution. In *IEEE Conference on Computer Vision and Pattern Recognition*, pages 1732–1741, 2019. 2

[22] Zongyao He and Zhi Jin. Latent modulated function for computational optimal continuous image representation. In *Proceedings of the IEEE/CVF Conference on Computer Vision and Pattern Recognition*, pages 26026–26035, 2024. 3, 7

[23] Jintong Hu, Bin Xia, Bin Chen, Wenming Yang, and Lei Zhang. Gaussiansr: High fidelity 2d gaussian splatting for arbitrary-scale image super-resolution. In *Proceedings of the Association for the Advancement of Artificial Intelligence*, 2025. 3, 7

[24] Xuecai Hu, Haoyuan Mu, Xiangyu Zhang, Zilei Wang, Tieniu Tan, and Jian Sun. Meta-sr: A magnification-arbitrary network for super-resolution. In *IEEE Conference on Computer Vision and Pattern Recognition*, pages 1575–1584, 2019. 2, 7

[25] Jia-Bin Huang, Abhishek Singh, and Narendra Ahuja. Single image super-resolution from transformed self-exemplars. In *IEEE Conference on Computer Vision and Pattern Recognition*, pages 5197–5206, 2015. 7

[26] Bernhard Kerbl, Georgios Kopanas, Thomas Leimkühler, and George Drettakis. 3d gaussian splatting for real-time radiance field rendering. *ACM Transaction on Graphics*, 42 (4):139–1, 2023. 2, 4

[27] Jiwon Kim, Jung Kwon Lee, and Kyoung Mu Lee. Accurate image super-resolution using very deep convolutional networks. In *IEEE Conference on Computer Vision and Pattern Recognition*, pages 1646–1654, 2016. 2

[28] Jiwon Kim, Jung Kwon Lee, and Kyoung Mu Lee. Deeply-recursive convolutional network for image super-resolution. In *IEEE Conference on Computer Vision and Pattern Recognition*, pages 1637–1645, 2016. 2

[29] Diederik P Kingma and Jimmy Ba. Adam: A method for stochastic optimization. *arXiv preprint arXiv:1412.6980*, 2014. 7

[30] Wei-Sheng Lai, Jia-Bin Huang, Narendra Ahuja, and Ming-Hsuan Yang. Deep laplacian pyramid networks for fast and accurate super-resolution. In *IEEE Conference on Computer Vision and Pattern Recognition*, pages 624–632, 2017. 2

[31] Christian Ledig, Lucas Theis, Ferenc Huszár, Jose Caballero, Andrew Cunningham, Alejandro Acosta, Andrew Aitken, Alykhan Tejani, Johannes Totz, Zehan Wang, et al. Photo-realistic single image super-resolution using a generative adversarial network. In *IEEE Conference on Computer Vision and Pattern Recognition*, pages 4681–4690, 2017. 2

[32] Jaewon Lee and Kyong Hwan Jin. Local texture estimator for implicit representation function. In *Proceedings of the IEEE/CVF Conference on Computer Vision and Pattern Recognition*, pages 1929–1938, 2022. 2, 3, 7

[33] Juncheng Li, Faming Fang, Kangfu Mei, and Guixu Zhang. Multi-scale residual network for image super-resolution. In *European Conference on Computer Vision*, pages 517–532, 2018. 2

[34] Wenbo Li, Kun Zhou, Lu Qi, Liying Lu, and Jiangbo Lu. Best-buddy gans for highly detailed image super-resolution. In *Proceedings of the AAAI Conference on Artificial Intelligence*, pages 1412–1420, 2022. 2

[35] Yawei Li, Yuchen Fan, Xiaoyu Xiang, Denis Demandolx, Rakesh Ranjan, Radu Timofte, and Luc Van Gool. Efficient and explicit modelling of image hierarchies for image restoration. In *Proceedings of the IEEE/CVF Conference*

*on Computer Vision and Pattern Recognition*, pages 18278–18289, 2023. 2

[36] Yawei Li, Kai Zhang, Jingyun Liang, Jiezhang Cao, Ce Liu, Rui Gong, Yulun Zhang, Hao Tang, Yun Liu, Denis Demandolx, et al. Lsdir: A large scale dataset for image restoration. In *Proceedings of the IEEE/CVF Conference on Computer Vision and Pattern Recognition*, pages 1775–1787, 2023. 5, 6, 7

[37] Zhen Li, Jinglei Yang, Zheng Liu, Xiaomin Yang, Gwanggil Jeon, and Wei Wu. Feedback network for image super-resolution. In *IEEE Conference on Computer Vision and Pattern Recognition*, pages 3867–3876, 2019. 1, 2

[38] Jingyun Liang, Jiezhang Cao, Guolei Sun, Kai Zhang, Luc Van Gool, and Radu Timofte. Swinir: Image restoration using swin transformer. In *Proceedings of the IEEE/CVF International Conference on Computer Vision Workshop*, pages 1833–1844, 2021. 1, 2

[39] Jie Liang, Hui Zeng, and Lei Zhang. Details or artifacts: A locally discriminative learning approach to realistic image super-resolution. In *IEEE Conference on Computer Vision and Pattern Recognition*, pages 5657–5666, 2022. 1, 2

[40] Bee Lim, Sanghyun Son, Heewon Kim, Seungjun Nah, and Kyoung Mu Lee. Enhanced deep residual networks for single image super-resolution. In *IEEE Conference on Computer Vision and Pattern Recognition Workshop*, pages 136–144, 2017. 2, 5, 6, 7, 9

[41] Xian Liu, Xiaohang Zhan, Jiaxiang Tang, Ying Shan, Gang Zeng, Dahua Lin, Xihui Liu, and Ziwei Liu. Humangaussian: Text-driven 3d human generation with gaussian splatting. In *IEEE/CVF Conference on Computer Vision and Pattern Recognition*, pages 6646–6657, 2024. 2

[42] Ze Liu, Yutong Lin, Yue Cao, Han Hu, Yixuan Wei, Zheng Zhang, Stephen Lin, and Baining Guo. Swin transformer: Hierarchical vision transformer using shifted windows. In *Proceedings of the IEEE/CVF international conference on computer vision*, pages 10012–10022, 2021. 2, 5

[43] Cheng Ma, Yongming Rao, Yean Cheng, Ce Chen, Jiwen Lu, and Jie Zhou. Structure-preserving super resolution with gradient guidance. In *Proceedings of the IEEE/CVF conference on computer vision and pattern recognition*, pages 7769–7778, 2020. 2

[44] Cheng Ma, Yongming Rao, Jiwen Lu, and Jie Zhou. Structure-preserving image super-resolution. *IEEE Transactions on Pattern Analysis and Machine Intelligence*, 44(11): 7898–7911, 2021. 2

[45] David Martin, Charless Fowlkes, Doron Tal, and Jitendra Malik. A database of human segmented natural images and its application to evaluating segmentation algorithms and measuring ecological statistics. In *IEEE International Conference on Computer Vision*, pages 416–423. IEEE, 2001. 7

[46] Yusuke Matsui, Kota Ito, Yuji Aramaki, Azuma Fujimoto, Toru Ogawa, Toshihiko Yamasaki, and Kiyoharu Aizawa. Sketch-based manga eetrieval using manga109 dataset. *Multimedia Tools and Applications*, 76(20):21811–21838, 2017. 7

[47] Yiqun Mei, Yuchen Fan, and Yuqian Zhou. Image super-resolution with non-local sparse attention. In *IEEE Conference on Computer Vision and Pattern Recognition*, pages 3517–3526, 2021. 2

[48] Ben Mildenhall, Pratul P Srinivasan, Matthew Tancik, Jonathan T Barron, Ravi Ramamoorthi, and Ren Ng. Nerf: Representing scenes as neural radiance fields for view synthesis. In *European Conference on Computer Vision*, pages 405–421, 2020. 1, 2, 3

[49] KL Navaneet, Kossar Pourahmadi Meibodi, Soroush Abbasi Koohpayegani, and Hamed Pirsiavash. Compgs: Smaller and faster gaussian splatting with vector quantization. In *European Conference on Computer Vision*, 2024. 2

[50] Byeonghyun Pak, Jaewon Lee, and Kyong Hwan Jin. B-spline texture coefficients estimator for screen content image super-resolution. In *Proceedings of the IEEE/CVF Conference on Computer Vision and Pattern Recognition*, pages 10062–10071, 2023. 3

[51] Seung Ho Park, Young Su Moon, and Nam Ik Cho. Perception-oriented single image super-resolution using optimal objective estimation. In *Proceedings of the IEEE/CVF Conference on Computer Vision and Pattern Recognition*, pages 1725–1735, 2023. 2

[52] Robin Rombach, Andreas Blattmann, Dominik Lorenz, Patrick Esser, and Björn Ommer. High-resolution image synthesis with latent diffusion models. In *Proceedings of the IEEE/CVF conference on computer vision and pattern recognition*, pages 10684–10695, 2022. 5

[53] Mehdi SM Sajjadi, Bernhard Scholkopf, and Michael Hirsch. Enhancenet: Single image super-resolution through automated texture synthesis. In *IEEE International Conference on Computer Vision*, pages 4491–4500, 2017. 2

[54] Wenzhe Shi, Jose Caballero, Ferenc Huszár, Johannes Totz, Andrew P Aitken, Rob Bishop, Daniel Rueckert, and Zehan Wang. Real-time single image and video super-resolution using an efficient sub-pixel convolutional neural network. In *Proceedings of the IEEE Conference on Computer Vision and Pattern Recognition*, pages 1874–1883, 2016. 1, 2

[55] Radu Timofte, Eirikur Agustsson, Luc Van Gool, Ming-Hsuan Yang, and Lei Zhang. Ntire 2017 challenge on single image super-resolution: Methods and results. In *IEEE Conference on Computer Vision and Pattern Recognition Workshop*, pages 114–125, 2017. 5, 6, 7

[56] Junjie Wang, Jiemin Fang, Xiaopeng Zhang, Lingxi Xie, and Qi Tian. Gaussianeditor: Editing 3d gaussians delicately with text instructions. In *PIEEE/CVF Conference on Computer Vision and Pattern Recognition*, pages 20902–20911, 2024. 2

[57] Jianyi Wang, Zongsheng Yue, Shangchen Zhou, Kelvin CK Chan, and Chen Change Loy. Exploiting diffusion prior for real-world image super-resolution. *International Journal of Computer Vision*, pages 1–21, 2024. 1, 2

[58] Longguang Wang, Yingqian Wang, Zaiping Lin, Jungang Yang, Wei An, and Yulan Guo. Learning a single network for scale-arbitrary super-resolution. In *Proceedings of the IEEE/CVF International Conference on Computer Vision*, pages 4801–4810, 2021. 3

[59] Xintao Wang, Ke Yu, Chao Dong, and Chen Change Loy. Recovering realistic texture in image super-resolution by

deep spatial feature transform. In *IEEE Conference on Computer Vision and Pattern Recognition*, pages 606–615, 2018. 2

[60] Xintao Wang, Ke Yu, Shixiang Wu, Jinjin Gu, Yihao Liu, Chao Dong, Yu Qiao, and Chen Change Loy. Esrgan: Enhanced super-resolution generative adversarial networks. In *European Conference on Computer Vision Workshop*, pages 0–0, 2018. 1

[61] Xintao Wang, Liangbin Xie, Chao Dong, and Ying Shan. Real-esrgan: Training real-world blind super-resolution with pure synthetic data. In *IEEE International Conference on Computer Vision*, pages 1905–1914, 2021. 1

[62] Yufei Wang, Wenhan Yang, Xinyuan Chen, Yaohui Wang, Lanqing Guo, Lap-Pui Chau, Ziwei Liu, Yu Qiao, Alex C Kot, and Bihan Wen. Sinsr: diffusion-based image super-resolution in a single step. In *IEEE/CVF Conference on Computer Vision and Pattern Recognition*, pages 25796–25805, 2024. 1, 2

[63] Zhou Wang, Alan C Bovik, Hamid R Sheikh, and Eero P Simoncelli. Image quality assessment: From error visibility to structural similarity. *IEEE Transactions on Image Processing*, 13(4):600–612, 2004. 7

[64] Min Wei and Xuesong Zhang. Super-resolution neural operator. In *Proceedings of the IEEE/CVF Conference on Computer Vision and Pattern Recognition*, pages 18247–18256, 2023. 3, 7

[65] Rongyuan Wu, Lingchen Sun, Zhiyuan Ma, and Lei Zhang. One-step effective diffusion network for real-world image super-resolution. In *Neural Information Processing Systems*, 2024. 1, 2

[66] Rongyuan Wu, Tao Yang, Lingchen Sun, Zhengqiang Zhang, Shuai Li, and Lei Zhang. SeeSR: Towards semantics-aware real-world image super-resolution. In *IEEE/CVF conference on Computer Vision and Pattern Recognition*, pages 25456–25467, 2024. 1, 2

[67] Jingyu Yang, Sheng Shen, Huanjing Yue, and Kun Li. Implicit transformer network for screen content image continuous super-resolution. *Advances in Neural Information Processing Systems*, 34:13304–13315, 2021. 3

[68] Sipeng Yang, Qingchuan Zhu, Junhao Zhuge, Qiang Qiu, Chen Li, Yuzhong Yan, Huihui Xu, Ling-Qi Yan, and Xiaogang Jin. Mob-fgsr: Frame generation and super resolution for mobile real-time rendering. In *ACM SIGGRAPH 2024 Conference Papers*, pages 1–11, 2024. 2

[69] Jie-En Yao, Li-Yuan Tsao, Yi-Chen Lo, Roy Tseng, Chia-Che Chang, and Chun-Yi Lee. Local implicit normalizing flow for arbitrary-scale image super-resolution. In *Proceedings of the IEEE/CVF Conference on Computer Vision and Pattern Recognition*, pages 1776–1785, 2023. 2, 3, 7

[70] Fanghua Yu, Jinjin Gu, Zheyuan Li, Jinfan Hu, Xiangtao Kong, Xintao Wang, Jingwen He, Yu Qiao, and Chao Dong. Scaling up to excellence: Practicing model scaling for photo-realistic image restoration in the wild. In *IEEE/CVF Conference on Computer Vision and Pattern Recognition*, pages 25669–25680, 2024. 1, 2

[71] Zongsheng Yue, Jianyi Wang, and Chen Change Loy. Resshift: Efficient diffusion model for image super-resolution by residual shifting. *Proceedings of the Advances in Neural Information Processing Systems*, 2023. 1, 2

[72] Roman Zeyde, Michael Elad, and Matan Protter. On single image scale-up using sparse-representations. In *International Conference on Curves and Surfaces*, pages 711–730. Springer, 2010. 7

[73] Kai Zhang, Jingyun Liang, Luc Van Gool, and Radu Timofte. Designing a practical degradation model for deep blind image super-resolution. In *IEEE International Conference on Computer Vision*, pages 4791–4800, 2021. 1, 2

[74] Leheng Zhang, Yawei Li, Xingyu Zhou, Xiaorui Zhao, and Shuhang Gu. Transcending the limit of local window: Advanced super-resolution transformer with adaptive token dictionary. In *Proceedings of the IEEE/CVF Conference on Computer Vision and Pattern Recognition*, pages 2856–2865, 2024. 1, 2

[75] Richard Zhang, Phillip Isola, Alexei A Efros, Eli Shechtman, and Oliver Wang. The unreasonable effectiveness of deep features as a perceptual metric. In *IEEE Conference on Computer Vision and Pattern Recognition*, pages 586–595, 2018. 7

[76] Wenlong Zhang, Yihao Liu, Chao Dong, and Yu Qiao. Ranksrgan: Generative adversarial networks with ranker for image super-resolution. In *Proceedings of the IEEE/CVF International Conference on Computer Vision*, pages 3096–3105, 2019. 2

[77] Xindong Zhang, Hui Zeng, Shi Guo, and Lei Zhang. Efficient long-range attention network for image super-resolution. In *European Conference on Computer Vision*, pages 649–667. Springer, 2022. 1, 2

[78] Xinjie Zhang, Xingtong Ge, Tongda Xu, Dailan He, Yan Wang, Hongwei Qin, Guo Lu, Jing Geng, and Jun Zhang. Gaussianimage: 1000 fps image representation and compression by 2d gaussian splatting. In *European Conference on Computer Vision*, pages 327–345, 2024. 2

[79] Yulun Zhang, Kunpeng Li, Kai Li, Lichen Wang, Bineng Zhong, and Yun Fu. Image super-resolution using very deep residual channel attention networks. In *European Conference on Computer Vision*, pages 286–301, 2018. 1, 2

[80] Yulun Zhang, Yapeng Tian, Yu Kong, Bineng Zhong, and Yun Fu. Residual dense network for image super-resolution. In *IEEE Conference on Computer Vision and Pattern Recognition*, pages 2472–2481, 2018. 1, 2, 6, 7, 8

[81] Lingzhe Zhao, Peng Wang, and Peidong Liu. Bad-gaussians: Bundle adjusted deblur gaussian splatting. In *European Conference on Computer Vision*, pages 233–250, 2024. 2

[82] Xizhou Zhu, Weijie Su, Lewei Lu, Bin Li, Xiaogang Wang, and Jifeng Dai. Deformable detr: Deformable transformers for end-to-end object detection. In *International Conference on Learning Representations*, 2021. 4

arXiv:2501.06838v1 [eess.IV] 12 Jan 2025

# Appendix to "Generalized and Efficient 2D Gaussian Splatting for Arbitrary-scale Super-Resolution"

In this appendix, we provide the following materials:

- More quantitative results on other testing datasets (please refer to Section 4.2 in the main paper);
- More qualitative results (please refer to Section 4.2 in the main paper);
- More results on the computational costs (please refer to Section 4.2 in the main paper);
- Ablation study (please refer to Section 4.2 in the main paper);

## 1. Quantitative Results

We compare our proposed GSASR with state-of-the-art (SoTA) methods, including Meta-SR [8], LIIF [3], LTE [10], SRNO [17], LINF [18], CiasoSR [2], LMF [6] and GaussianSR [7]. In Sec. 4.1 of the main paper, we have reported the results on DIV2K100 [15] and LSDIR [11] datasets. Here we report the results on the widely-used Set5 [1], Set14 [19], Urban100 [9], BSDS100 [13], Manga109 [14], General100 [5] testing sets. For the performance measures, we report PSNR, SSIM [16], LPIPS [20], and DISTS [4] indices. The PSNR and SSIM [16] are computed in the Y channel of Ycbcr space. The results are presented in Tabs. 1, 2, 3, 4, 5, 6.

Table 1. Quantitative results of representative ASR models and our proposed GSASR. All models use the same EDSR-backbone [12] as the feature extraction encoder. We test on Urban100 [9] and Manga109 [14] with scaling factors $\times 2$, $\times 3$, $\times 4$, $\times 6$, $\times 8$, $\times 12$. The best results are highlighted in red. The PSNR and SSIM [16] indices are computed in the Y channel of Ycbcr space.

| Scale | Metrics | Backbone: EDSR-baseline | | | | | | | | | | | | | | | | | |
|---|---|---|---|---|---|---|---|---|---|---|---|---|---|---|---|---|---|---|---|
| | | Testing Dataset: Urban100 | | | | | | | | | Testing Dataset: Manga109 | | | | | | | | |
| | | Meta -SR | LIIF | LTE | SRNO | LINF | LMF | Ciao -SR | Gaussian -SR | GSASR | Meta -SR | LIIF | LTE | SRNO | LINF | LMF | Ciao -SR | Gaussian -SR | GSASR |
| $\times 2$ | PSNR | 32.05 | 32.12 | 32.26 | 32.56 | 32.12 | 32.48 | 32.79 | 32.22 | 33.27 | 38.41 | 38.55 | 38.52 | 38.92 | 38.72 | 38.75 | 39.16 | 38.55 | 39.06 |
| | SSIM | 0.9280 | 0.9288 | 0.9299 | 0.9324 | 0.9283 | 0.9323 | 0.9344 | 0.9296 | 0.9389 | 0.9769 | 0.9770 | 0.9770 | 0.9778 | 0.9773 | 0.9774 | 0.9781 | 0.9771 | 0.9782 |
| | LPIPS | 0.0659 | 0.0643 | 0.0629 | 0.0597 | 0.0660 | 0.0603 | 0.0580 | 0.0590 | 0.0525 | 0.0239 | 0.0238 | 0.0229 | 0.0229 | 0.0239 | 0.0227 | 0.0224 | 0.0237 | 0.0209 |
| | DISTS | 0.0712 | 0.0717 | 0.0711 | 0.0692 | 0.0717 | 0.0696 | 0.0676 | 0.0712 | 0.0634 | 0.0226 | 0.0229 | 0.0234 | 0.0227 | 0.0231 | 0.0228 | 0.0222 | 0.0233 | 0.0215 |
| $\times 3$ | PSNR | 28.10 | 28.20 | 28.31 | 28.54 | 28.21 | 28.59 | 28.67 | 28.27 | 29.17 | 33.49 | 33.46 | 33.54 | 33.88 | 33.57 | 33.73 | 33.92 | 33.55 | 34.10 |
| | SSIM | 0.8520 | 0.8544 | 0.8561 | 0.8599 | 0.8538 | 0.8615 | 0.8627 | 0.8553 | 0.8733 | 0.9442 | 0.9449 | 0.9454 | 0.9470 | 0.9453 | 0.9467 | 0.9474 | 0.9452 | 0.9500 |
| | LPIPS | 0.1591 | 0.1542 | 0.1513 | 0.1465 | 0.1570 | 0.1437 | 0.1408 | 0.1541 | 0.1320 | 0.0669 | 0.0652 | 0.0643 | 0.0624 | 0.0652 | 0.0618 | 0.0601 | 0.0656 | 0.0604 |
| | DISTS | 0.1277 | 0.1290 | 0.1278 | 0.1243 | 0.1291 | 0.1250 | 0.1181 | 0.1288 | 0.1156 | 0.0505 | 0.0528 | 0.0536 | 0.0515 | 0.0522 | 0.0515 | 0.0477 | 0.0544 | 0.0487 |
| $\times 4$ | PSNR | 25.94 | 26.14 | 26.24 | 26.48 | 26.16 | 26.50 | 26.69 | 26.19 | 27.01 | 30.37 | 30.54 | 30.58 | 30.83 | 30.52 | 30.76 | 30.99 | 30.54 | 31.16 |
| | SSIM | 0.7824 | 0.7885 | 0.7910 | 0.7976 | 0.7878 | 0.7985 | 0.8031 | 0.7893 | 0.8142 | 0.9063 | 0.9097 | 0.9108 | 0.9137 | 0.9104 | 0.9130 | 0.9160 | 0.9094 | 0.9194 |
| | LPIPS | 0.2367 | 0.2271 | 0.2223 | 0.2136 | 0.2308 | 0.2151 | 0.2078 | 0.2283 | 0.1987 | 0.1112 | 0.1072 | 0.1064 | 0.1017 | 0.1079 | 0.1032 | 0.0991 | 0.1085 | 0.0990 |
| | DISTS | 0.1683 | 0.1738 | 0.1718 | 0.1679 | 0.1748 | 0.1696 | 0.1659 | 0.1730 | 0.1552 | 0.0735 | 0.0814 | 0.0831 | 0.0804 | 0.0818 | 0.0804 | 0.0802 | 0.0831 | 0.0749 |
| $\times 6$ | PSNR | 23.57 | 23.78 | 23.84 | 24.07 | 23.79 | 24.08 | 24.23 | 23.77 | 24.51 | 26.26 | 26.73 | 26.85 | 27.05 | 26.71 | 26.95 | 27.16 | 26.63 | 27.36 |
| | SSIM | 0.6726 | 0.6850 | 0.6872 | 0.6956 | 0.6836 | 0.6968 | 0.7029 | 0.6814 | 0.7165 | 0.8214 | 0.8378 | 0.8401 | 0.8455 | 0.8376 | 0.9428 | 0.8486 | 0.8333 | 0.8539 |
| | LPIPS | 0.3540 | 0.3355 | 0.3431 | 0.3292 | 0.3425 | 0.3327 | 0.3117 | 0.3499 | 0.2975 | 0.2024 | 0.1853 | 0.1883 | 0.1784 | 0.1859 | 0.1840 | 0.1693 | 0.1942 | 0.1680 |
| | DISTS | 0.2312 | 0.2354 | 0.2320 | 0.2258 | 0.2374 | 0.2300 | 0.2250 | 0.2364 | 0.2111 | 0.1182 | 0.1255 | 0.1240 | 0.1208 | 0.1265 | 0.1215 | 0.1235 | 0.1271 | 0.1169 |
| $\times 8$ | PSNR | 22.27 | 22.45 | 22.53 | 22.69 | 22.45 | 22.73 | 22.83 | 22.36 | 23.09 | 24.06 | 24.53 | 24.63 | 24.78 | 24.51 | 24.71 | 24.93 | 24.26 | 25.09 |
| | SSIM | 0.6004 | ¥0.6169 | 0.6190 | 0.6269 | 0.6141 | 0.6286 | 0.6344 | 0.6070 | 0.6480 | 0.7529 | 0.7786 | 0.7810 | 0.7871 | 0.7779 | 0.7837 | 0.7933 | 0.7657 | 0.7981 |
| | LPIPS | 0.4536 | ¥0.4201 | 0.4341 | 0.4168 | 0.4301 | 0.4205 | 0.3932 | 0.4530 | 0.3754 | 0.2989 | 0.2603 | 0.2677 | 0.2533 | 0.2595 | 0.2620 | 0.2343 | 0.2868 | 0.2304 |
| | DISTS | 0.2765 | ¥0.2795 | 0.2763 | 0.2698 | 0.2831 | 0.2748 | 0.2666 | 0.2883 | 0.2515 | 0.1576 | 0.1630 | 0.1603 | 0.1559 | 0.1640 | 0.1584 | 0.1565 | 0.1714 | 0.1480 |
| $\times 12$ | PSNR | 20.77 | 20.89 | 20.96 | 21.10 | 20.88 | 21.12 | 21.19 | 20.68 | 21.39 | 21.71 | 22.05 | 22.13 | 22.22 | 22.02 | 22.17 | 22.34 | 21.63 | 22.43 |
| | SSIM | 0.5191 | 0.5370 | 0.5383 | 0.5454 | 0.5337 | 0.5460 | 0.5530 | 0.5217 | 0.5628 | 0.6655 | 0.6967 | 0.6982 | 0.7029 | 0.6953 | 0.7001 | 0.7124 | 0.6745 | 0.7147 |
| | LPIPS | 0.5818 | 0.5540 | 0.5729 | 0.5544 | 0.5676 | 0.5405 | 0.5204 | 0.6198 | 0.4994 | 0.4324 | 0.3931 | 0.4046 | 0.3897 | 0.3900 | 0.3973 | 0.3540 | 0.4508 | 0.3433 |
| | DISTS | 0.3397 | 0.3421 | 0.3399 | 0.3333 | 0.3479 | 0.3388 | 0.3278 | 0.3646 | 0.3135 | 0.2201 | 0.2252 | 0.2215 | 0.2168 | 0.2271 | 0.2205 | 0.2145 | 0.2466 | 0.2014 |

From the quantitative results, one could find that GSASR significantly outperforms other arbitrary-scale super-resolution models in most benchmarks. GSASR drops slightly under high scaling factors (such as $\times 12$). This is because its performance

Table 2. Quantitative results of representative ASR models and our proposed GSASR. All models use the same RDN backbone [21] as the feature extraction encoder. We test on Urban100 [9] and Manga109 [14] with scaling factors ×2, ×3, ×4, ×6, ×8, ×12. The best results are highlighted in red. The PSNR and SSIM [16] indices are computed in the Y channel of Ycbcr space.

| Scale | Metrics | Backbone: RDN | | | | | | | | | | | | | | | | | | |
|---|---|---|---|---|---|---|---|---|---|---|---|---|---|---|---|---|---|---|---|---|
| | | Testing Dataset: Urban100 | | | | | | | | | Testing Dataset: Manga109 | | | | | | | | | |
| | | Meta -SR | LIIF | LTE | SRNO | LINF | LMF | Ciao -SR | Gaussian -SR | GSASR | Meta -SR | LIIF | LTE | SRNO | LINF | LMF | Ciao -SR | Gaussian -SR | GSASR |
| ×2 | PSNR | 33.04 | 32.84 | 33.00 | 33.27 | 32.87 | 33.08 | 33.30 | 32.96 | 33.53 | 39.34 | 39.04 | 39.08 | 39.35 | 39.23 | 39.24 | 39.55 | 39.16 | 39.17 |
| | SSIM | 0.9363 | 0.9353 | 0.9365 | 0.9390 | 0.9350 | 0.9371 | 0.9388 | 0.9363 | 0.9406 | 0.9783 | 0.9782 | 0.9781 | 0.9785 | 0.9784 | 0.9784 | 0.9789 | 0.9781 | 0.9784 |
| | LPIPS | 0.0552 | 0.0569 | 0.0552 | 0.0518 | 0.0569 | 0.0557 | 0.0534 | 0.0563 | 0.0507 | 0.0227 | 0.0231 | 0.0223 | 0.0218 | 0.0228 | 0.0229 | 0.0218 | 0.0230 | 0.0209 |
| | DISTS | 0.0666 | 0.0666 | 0.0660 | 0.0640 | 0.0671 | 0.0659 | 0.0638 | 0.0665 | 0.0617 | 0.0224 | 0.0218 | 0.0221 | 0.0218 | 0.0222 | 0.0222 | 0.0216 | 0.0222 | 0.0213 |
| ×3 | PSNR | 28.94 | 28.81 | 28.96 | 29.12 | 28.82 | 29.11 | 29.17 | 28.93 | 29.35 | 34.40 | 34.11 | 34.26 | 34.58 | 34.25 | 34.36 | 34.61 | 34.29 | 34.26 |
| | SSIM | 0.8677 | 0.8664 | 0.8686 | 0.8714 | 0.8658 | 0.8709 | 0.8716 | 0.8680 | 0.8760 | 0.9492 | 0.9487 | 0.9492 | 0.9507 | 0.9489 | 0.9499 | 0.9509 | 0.9493 | 0.9507 |
| | LPIPS | 0.1381 | 0.1382 | 0.1373 | 0.1332 | 0.1399 | 0.1335 | 0.1334 | 0.1384 | 0.1294 | 0.0622 | 0.0620 | 0.0612 | 0.0598 | 0.0617 | 0.0598 | 0.0592 | 0.0616 | 0.0596 |
| | DISTS | 0.1194 | 0.1194 | 0.1186 | 0.1158 | 0.1208 | 0.1167 | 0.1134 | 0.1196 | 0.1126 | 0.0509 | 0.0504 | 0.0508 | 0.0496 | 0.0502 | 0.0498 | 0.0483 | 0.0509 | 0.0488 |
| ×4 | PSNR | 26.71 | 26.67 | 26.80 | 26.97 | 26.69 | 26.94 | 27.10 | 26.77 | 27.15 | 31.33 | 31.15 | 31.27 | 31.56 | 31.19 | 31.41 | 31.61 | 31.27 | 31.31 |
| | SSIM | 0.8055 | 0.8041 | 0.8074 | 0.8119 | 0.8039 | 0.8104 | 0.8142 | 0.8064 | 0.8177 | 0.9177 | 0.9169 | 0.9180 | 0.9208 | 0.9173 | 0.9195 | 0.9216 | 0.9180 | 0.9208 |
| | LPIPS | 0.2062 | 0.2077 | 0.2047 | 0.1987 | 0.2090 | 0.2020 | 0.1966 | 0.2069 | 0.1953 | 0.1001 | 0.1003 | 0.0995 | 0.0970 | 0.1006 | 0.0980 | 0.0957 | 0.0999 | 0.0973 |
| | DISTS | 0.1562 | 0.1612 | 0.1600 | 0.1563 | 0.1636 | 0.1589 | 0.1559 | 0.1610 | 0.1515 | 0.0747 | 0.0778 | 0.0786 | 0.0773 | 0.0788 | 0.0773 | 0.0775 | 0.0782 | 0.0747 |
| ×6 | PSNR | 24.07 | 24.19 | 24.27 | 24.42 | 24.18 | 24.39 | 24.58 | 24.16 | 24.63 | 27.09 | 27.30 | 27.48 | 27.70 | 27.31 | 27.52 | 27.70 | 27.24 | 27.59 |
| | SSIM | 0.6966 | 0.7028 | 0.7058 | 0.7113 | 0.7010 | 0.7102 | 0.7173 | 0.6996 | 0.7214 | 0.8426 | 0.8507 | 0.8531 | 0.8572 | 0.8502 | 0.8537 | 0.8585 | 0.8470 | 0.8582 |
| | LPIPS | 0.3158 | 0.3099 | 0.3220 | 0.3148 | 0.3155 | 0.3169 | 0.2950 | 0.3241 | 0.2943 | 0.1720 | 0.1687 | 0.1746 | 0.1888 | 0.1718 | 0.1732 | 0.1616 | 0.1758 | 0.1638 |
| | DISTS | 0.2084 | 0.2176 | 0.2160 | 0.2110 | 0.2217 | 0.2149 | 0.2111 | 0.2191 | 0.2064 | 0.1063 | 0.1184 | 0.1171 | 0.1160 | 0.1209 | 0.1155 | 0.1201 | 0.1175 | 0.1141 |
| ×8 | PSNR | 22.64 | 22.78 | 22.86 | 23.01 | 22.77 | 22.97 | 23.13 | 22.64 | 23.19 | 24.64 | 25.02 | 25.11 | 25.30 | 24.99 | 25.16 | 25.40 | 24.62 | 25.27 |
| | SSIM | 0.6213 | 0.6338 | 0.6362 | 0.6423 | 0.6305 | 0.6408 | 0.6484 | 0.6234 | 0.6522 | 0.7746 | 0.7947 | 0.7961 | 0.8014 | 0.7925 | 0.7968 | 0.8057 | 0.7794 | 0.8034 |
| | LPIPS | 0.4022 | 0.3903 | 0.4107 | 0.4011 | 0.4010 | 0.4037 | 0.3733 | 0.4249 | 0.3723 | 0.2501 | 0.2342 | 0.2480 | 0.2390 | 0.2391 | 0.2460 | 0.2218 | 0.2631 | 0.2244 |
| | DISTS | 0.2512 | 0.2591 | 0.2586 | 0.2520 | 0.2657 | 0.2580 | 0.2507 | 0.2704 | 0.2460 | 0.1371 | 0.1503 | 0.1503 | 0.1480 | 0.1550 | 0.1492 | 0.1503 | 0.1575 | 0.1433 |
| ×12 | PSNR | 21.00 | 21.15 | 21.22 | 21.35 | 21.12 | 21.33 | 21.44 | 20.84 | 21.47 | 22.03 | 22.38 | 22.45 | 22.58 | 22.32 | 22.48 | 22.67 | 21.76 | 22.58 |
| | SSIM | 0.5317 | 0.5499 | 0.5514 | 0.5571 | 0.5462 | 0.5561 | 0.5637 | 0.5319 | 0.5670 | 0.6804 | 0.7115 | 0.7116 | 0.7165 | 0.7073 | 0.7121 | 0.7247 | 0.6834 | 0.7209 |
| | LPIPS | 0.5332 | 0.5198 | 0.5477 | 0.5374 | 0.5365 | 0.5403 | 0.5005 | 0.5929 | 0.4927 | 0.3830 | 0.3597 | 0.3809 | 0.3686 | 0.3670 | 0.3772 | 0.3352 | 0.4281 | 0.3370 |
| | DISTS | 0.3144 | 0.3209 | 0.3216 | 0.3149 | 0.3304 | 0.3216 | 0.3114 | 0.3485 | 0.3072 | 0.1972 | 0.2076 | 0.2082 | 0.2038 | 0.2156 | 0.2077 | 0.2043 | 0.2329 | 0.1958 |

Table 3. Quantitative results of representative ASR models and our proposed GSASR. All models use the same EDSR-backbone [12] as the feature extraction encoder. We test on BSDS100 [13] and General100 [5] with scaling factors ×2, ×3, ×4, ×6, ×8, ×12. The best results are highlighted in red. The PSNR and SSIM [16] indices are computed in the Y channel of Ycbcr space.

| Scale | Metrics | Backbone: EDSR-baseline | | | | | | | | | | | | | | | | | | |
|---|---|---|---|---|---|---|---|---|---|---|---|---|---|---|---|---|---|---|---|---|
| | | Testing Dataset: BSDS100 | | | | | | | | | Testing Dataset: General100 | | | | | | | | | |
| | | Meta -SR | LIIF | LTE | SRNO | LINF | LMF | Ciao -SR | Gaussian -SR | GSASR | Meta -SR | LIIF | LTE | SRNO | LINF | LMF | Ciao -SR | Gaussian -SR | GSASR |
| ×2 | PSNR | 32.13 | 32.14 | 32.17 | 32.23 | 32.16 | 32.21 | 32.28 | 32.17 | 32.39 | 38.01 | 38.04 | 38.10 | 38.25 | 38.27 | 38.18 | 38.47 | 38.10 | 38.61 |
| | SSIM | 0.8994 | 0.8994 | 0.8997 | 0.9007 | 0.8989 | 0.9004 | 0.9007 | 0.8998 | 0.9023 | 0.9611 | 0.9612 | 0.9615 | 0.9622 | 0.9613 | 0.9619 | 0.9624 | 0.9615 | 0.9632 |
| | LPIPS | 0.1484 | 0.1479 | 0.1462 | 0.1452 | 0.1520 | 0.1430 | 0.1462 | 0.1480 | 0.1370 | 0.0441 | 0.0435 | 0.0429 | 0.0424 | 0.0447 | 0.0416 | 0.0423 | 0.0440 | 0.0385 |
| | DISTS | 0.1043 | 0.1045 | 0.1045 | 0.1031 | 0.1044 | 0.1043 | 0.1019 | 0.1042 | 0.1004 | 0.0587 | 0.0589 | 0.0590 | 0.0574 | 0.0585 | 0.0583 | 0.0573 | 0.0590 | 0.0544 |
| ×3 | PSNR | 29.07 | 29.08 | 29.12 | 29.17 | 29.12 | 29.16 | 29.19 | 29.12 | 29.32 | 33.82 | 33.87 | 33.93 | 34.07 | 33.99 | 34.01 | 34.14 | 33.92 | 34.38 |
| | SSIM | 0.8055 | 0.8062 | 0.8065 | 0.8076 | 0.8056 | 0.8081 | 0.8076 | 0.8065 | 0.8121 | 0.9111 | 0.9118 | 0.9122 | 0.9135 | 0.9120 | 0.9133 | 0.9136 | 0.9121 | 0.9169 |
| | LPIPS | 0.2884 | 0.2819 | 0.2800 | 0.2793 | 0.2867 | 0.2738 | 0.2782 | 0.2819 | 0.2710 | 0.1164 | 0.1128 | 0.1121 | 0.1108 | 0.1142 | 0.1076 | 0.1090 | 0.1137 | 0.1040 |
| | DISTS | 0.1637 | 0.1639 | 0.1639 | 0.1632 | 0.1639 | 0.1630 | 0.1597 | 0.1644 | 0.1592 | 0.1060 | 0.1067 | 0.1069 | 0.1044 | 0.1059 | 0.1043 | 0.1026 | 0.1075 | 0.1000 |
| ×4 | PSNR | 27.54 | 27.59 | 27.61 | 27.66 | 27.61 | 27.65 | 27.70 | 27.60 | 27.81 | 31.34 | 31.47 | 31.53 | 31.66 | 31.55 | 31.58 | 31.56 | 31.49 | 31.90 |
| | SSIM | 0.7355 | 0.7373 | 0.7379 | 0.7403 | 0.7373 | 0.7397 | 0.7411 | 0.7375 | 0.7460 | 0.8616 | 0.8637 | 0.8643 | 0.8669 | 0.8640 | 0.8657 | 0.8667 | 0.8638 | 0.8720 |
| | LPIPS | 0.3795 | 0.3717 | 0.3703 | 0.3635 | 0.3743 | 0.3664 | 0.3620 | 0.3736 | 0.3597 | 0.1829 | 0.1776 | 0.1769 | 0.1733 | 0.1791 | 0.1730 | 0.1723 | 0.1794 | 0.1654 |
| | DISTS | 0.2025 | 0.2037 | 0.2042 | 0.2040 | 0.2040 | 0.2032 | 0.2033 | 0.2045 | 0.1982 | 0.1457 | 0.1479 | 0.1479 | 0.1456 | 0.1479 | 0.1459 | 0.1470 | 0.1487 | 0.1383 |
| ×6 | PSNR | 25.74 | 25.83 | 25.86 | 25.90 | 25.85 | 25.89 | 25.95 | 25.82 | 26.04 | 28.39 | 28.64 | 28.70 | 28.78 | 28.69 | 28.70 | 28.89 | 28.59 | 29.02 |
| | SSIM | 0.6440 | 0.6489 | 0.6495 | 0.6522 | 0.6489 | 0.6512 | 0.6536 | 0.6465 | 0.6592 | 0.7793 | 0.7858 | 0.7868 | 0.7904 | 0.7858 | 0.7869 | 0.7922 | 0.7834 | 0.7977 |
| | LPIPS | 0.4948 | 0.4838 | 0.4919 | 0.4827 | 0.4888 | 0.4869 | 0.4763 | 0.4982 | 0.4702 | 0.2822 | 0.2705 | 0.2764 | 0.2695 | 0.2747 | 0.2734 | 0.2622 | 0.2833 | 0.2539 |
| | DISTS | 0.2586 | 0.2603 | 0.2605 | 0.2587 | 0.2596 | 0.2591 | 0.2588 | 0.2601 | 0.2532 | 0.2026 | 0.2056 | 0.2060 | 0.2032 | 0.2054 | 0.2039 | 0.2033 | 0.2075 | 0.1948 |
| ×8 | PSNR | 24.68 | 24.78 | 24.81 | 24.87 | 24.80 | 24.60 | 24.89 | 24.72 | 24.99 | 26.64 | 26.91 | 26.97 | 27.04 | 26.95 | 26.96 | 27.16 | 26.73 | 27.22 |
| | SSIM | 0.5894 | 0.5963 | 0.5966 | 0.5998 | 0.5960 | 0.5864 | 0.6013 | 0.5910 | 0.6065 | 0.7202 | 0.7300 | 0.7311 | 0.7345 | 0.7296 | 0.7315 | 0.7370 | 0.7233 | 0.7417 |
| | LPIPS | 0.5713 | 0.5526 | 0.5667 | 0.5564 | 0.5602 | 0.5771 | 0.5457 | 0.5770 | 0.5402 | 0.3648 | 0.3400 | 0.3524 | 0.3428 | 0.3449 | 0.3480 | 0.3304 | 0.3647 | 0.3220 |
| | DISTS | 0.2965 | 0.2992 | 0.3010 | 0.2981 | 0.2990 | 0.2945 | 0.2976 | 0.3015 | 0.2913 | 0.2414 | 0.2467 | 0.2478 | 0.2445 | 0.2466 | 0.2454 | 0.2439 | 0.2519 | 0.2348 |
| ×12 | PSNR | 23.42 | 23.51 | 23.54 | 23.57 | 23.53 | 23.56 | 23.61 | 23.37 | 23.62 | 24.45 | 24.69 | 24.77 | 24.83 | 24.71 | 24.76 | 24.94 | 24.33 | 24.85 |
| | SSIM | 0.5355 | 0.5437 | 0.5437 | 0.5457 | 0.5431 | 0.5447 | 0.5479 | 0.5358 | 0.5512 | 0.6454 | 0.6590 | 0.6602 | 0.6622 | 0.6581 | 0.6607 | 0.6662 | 0.6472 | 0.6693 |
| | LPIPS | 0.6580 | 0.6475 | 0.6664 | 0.6568 | 0.6575 | 0.6598 | 0.6397 | 0.6941 | 0.6302 | 0.4735 | 0.4527 | 0.4694 | 0.4629 | 0.4578 | 0.4624 | 0.4374 | 0.5033 | 0.4252 |
| | DISTS | 0.3482 | 0.3512 | 0.3548 | 0.3521 | 0.3529 | 0.3521 | 0.3498 | 0.3608 | 0.3419 | 0.2936 | 0.3006 | 0.3042 | 0.3017 | 0.3020 | 0.3007 | 0.2986 | 0.3140 | 0.2869 |

Table 4. Quantitative results of representative ASR models and our proposed GSASR. All models use the same RDN backbone [22] as the feature extraction encoder. We test on BSDS100 [13] and General100 [5] with scaling factors $\times 2$, $\times 3$, $\times 4$, $\times 6$, $\times 8$, $\times 12$. The best results are highlighted in red. The PSNR and SSIM [16] indices are computed in the Y channel of Ycbcr space.

| Scale | Metrics | Backbone: RDN | | | | | | | | | | | | | | | | | |
|---|---|---|---|---|---|---|---|---|---|---|---|---|---|---|---|---|---|---|---|
| | | Testing Dataset: BSDS100 | | | | | | | | | Testing Dataset: General100 | | | | | | | | |
| | | Meta -SR | LIIF | LTE | SRNO | LINF | LMF | Ciao -SR | Gaussian -SR | GSASR | Meta -SR | LIIF | LTE | SRNO | LINF | LMF | Ciao -SR | Gaussian -SR | GSASR |
| $\times 2$ | PSNR | 32.37 | 32.28 | 32.32 | 32.37 | 32.31 | 32.34 | 32.40 | 32.32 | 32.43 | 38.63 | 38.30 | 38.39 | 38.53 | 38.58 | 38.45 | 38.74 | 38.41 | 38.72 |
| | SSIM | 0.9012 | 0.9011 | 0.9015 | 0.9026 | 0.9012 | 0.9019 | 0.9022 | 0.9014 | 0.9029 | 0.9628 | 0.9626 | 0.9628 | 0.9636 | 0.9627 | 0.9631 | 0.9634 | 0.9628 | 0.9637 |
| | LPIPS | 0.1397 | 0.1455 | 0.1431 | 0.1385 | 0.1463 | 0.1427 | 0.1414 | 0.1453 | 0.1367 | 0.0405 | 0.0419 | 0.0413 | 0.0398 | 0.0424 | 0.0414 | 0.0409 | 0.0420 | 0.0382 |
| | DISTS | 0.1026 | 0.1016 | 0.1017 | 0.1011 | 0.1013 | 0.1025 | 0.1004 | 0.1020 | 0.0992 | 0.0572 | 0.0566 | 0.0560 | 0.0555 | 0.0566 | 0.0568 | 0.0556 | 0.0566 | 0.0540 |
| $\times 3$ | PSNR | 29.29 | 29.25 | 29.28 | 29.33 | 29.26 | 29.29 | 29.34 | 29.28 | 29.36 | 34.38 | 34.21 | 34.29 | 34.43 | 34.33 | 34.34 | 34.49 | 34.31 | 34.48 |
| | SSIM | 0.8095 | 0.8099 | 0.8103 | 0.8115 | 0.8096 | 0.8113 | 0.8113 | 0.8102 | 0.8131 | 0.9155 | 0.9154 | 0.9157 | 0.9171 | 0.9154 | 0.9165 | 0.9169 | 0.9160 | 0.9178 |
| | LPIPS | 0.2761 | 0.2782 | 0.2750 | 0.2717 | 0.2797 | 0.2708 | 0.2747 | 0.2774 | 0.2706 | 0.1075 | 0.1077 | 0.1075 | 0.1050 | 0.1089 | 0.1048 | 0.1053 | 0.1080 | 0.1032 |
| | DISTS | 0.1623 | 0.1613 | 0.1614 | 0.1609 | 0.1606 | 0.1605 | 0.1591 | 0.1619 | 0.1578 | 0.1041 | 0.1034 | 0.1026 | 0.1015 | 0.1031 | 0.1017 | 0.1009 | 0.1033 | 0.0997 |
| $\times 4$ | PSNR | 27.76 | 27.73 | 27.76 | 27.81 | 27.75 | 27.78 | 27.83 | 27.76 | 27.84 | 31.89 | 31.80 | 31.99 | 32.02 | 31.88 | 31.91 | 31.85 | 31.87 | 32.00 |
| | SSIM | 0.7424 | 0.7422 | 0.7430 | 0.7449 | 0.7422 | 0.7439 | 0.7453 | 0.7429 | 0.7471 | 0.8697 | 0.8692 | 0.8702 | 0.8724 | 0.8695 | 0.8708 | 0.8716 | 0.8701 | 0.8735 |
| | LPIPS | 0.3651 | 0.3646 | 0.3628 | 0.3576 | 0.3651 | 0.3614 | 0.3597 | 0.3652 | 0.3597 | 0.1692 | 0.1698 | 0.1690 | 0.1655 | 0.1708 | 0.1676 | 0.1669 | 0.1693 | 0.1642 |
| | DISTS | 0.2005 | 0.2016 | 0.2008 | 0.2007 | 0.2013 | 0.2007 | 0.2002 | 0.2011 | 0.1970 | 0.1420 | 0.1435 | 0.1422 | 0.1407 | 0.1429 | 0.1478 | 0.1423 | 0.1427 | 0.1367 |
| $\times 6$ | PSNR | 25.93 | 25.97 | 25.99 | 26.03 | 26.00 | 26.02 | 26.08 | 25.97 | 26.07 | 28.84 | 28.92 | 28.99 | 29.10 | 28.97 | 29.00 | 29.18 | 28.94 | 29.11 |
| | SSIM | 0.6521 | 0.6549 | 0.6556 | 0.6575 | 0.6548 | 0.6562 | 0.6587 | 0.6529 | 0.6607 | 0.7910 | 0.7936 | 0.7954 | 0.7979 | 0.7940 | 0.7952 | 0.7996 | 0.7928 | 0.8000 |
| | LPIPS | 0.4764 | 0.4726 | 0.4821 | 0.4756 | 0.4793 | 0.4809 | 0.4707 | 0.4863 | 0.4714 | 0.2591 | 0.2562 | 0.2648 | 0.2577 | 0.2618 | 0.2636 | 0.2536 | 0.2673 | 0.2521 |
| | DISTS | 0.2524 | 0.2562 | 0.2556 | 0.2544 | 0.2559 | 0.2551 | 0.2554 | 0.2551 | 0.2513 | 0.1931 | 0.1990 | 0.1985 | 0.1959 | 0.1998 | 0.1977 | 0.1975 | 0.1985 | 0.1929 |
| $\times 8$ | PSNR | 24.84 | 24.90 | 24.94 | 24.97 | 24.93 | 24.80 | 25.00 | 24.84 | 25.01 | 26.97 | 27.18 | 27.22 | 27.31 | 27.21 | 27.22 | 27.39 | 27.00 | 27.30 |
| | SSIM | 0.5965 | 0.6020 | 0.6025 | 0.6045 | 0.6014 | 0.5968 | 0.6058 | 0.5968 | 0.6080 | 0.7307 | 0.7382 | 0.7394 | 0.7423 | 0.7374 | 0.7397 | 0.7440 | 0.7322 | 0.7442 |
| | LPIPS | 0.5460 | 0.5409 | 0.5578 | 0.5509 | 0.5521 | 0.5707 | 0.5409 | 0.5650 | 0.5416 | 0.3319 | 0.3232 | 0.3406 | 0.3315 | 0.3327 | 0.3383 | 0.3214 | 0.3482 | 0.3200 |
| | DISTS | 0.2894 | 0.2945 | 0.2962 | 0.2943 | 0.2950 | 0.2940 | 0.2943 | 0.2959 | 0.2900 | 0.2299 | 0.2381 | 0.2398 | 0.2371 | 0.2404 | 0.2387 | 0.2377 | 0.2420 | 0.2327 |
| $\times 12$ | PSNR | 23.50 | 23.61 | 23.64 | 23.66 | 23.62 | 23.64 | 23.70 | 23.44 | 23.66 | 24.66 | 24.93 | 24.97 | 25.03 | 24.92 | 24.97 | 25.13 | 24.50 | 24.90 |
| | SSIM | 0.5395 | 0.5476 | 0.5478 | 0.5490 | 0.5465 | 0.5480 | 0.5512 | 0.5389 | 0.5528 | 0.6529 | 0.6666 | 0.6671 | 0.6693 | 0.6648 | 0.6675 | 0.6725 | 0.6533 | 0.6717 |
| | LPIPS | 0.6306 | 0.6350 | 0.6582 | 0.6517 | 0.6508 | 0.6519 | 0.6345 | 0.6823 | 0.6334 | 0.4393 | 0.4311 | 0.4578 | 0.4476 | 0.4451 | 0.4514 | 0.4255 | 0.4871 | 0.4220 |
| | DISTS | 0.3403 | 0.3461 | 0.3505 | 0.3493 | 0.3491 | 0.3493 | 0.3478 | 0.3536 | 0.3418 | 0.2807 | 0.2926 | 0.2989 | 0.2953 | 0.2964 | 0.2954 | 0.2933 | 0.3046 | 0.2850 |

Table 5. Quantitative results of representative ASR models and our proposed GSASR. All models use the same EDSR-backbone [12] as the feature extraction encoder. We test on Set5 [1] and Set14 [19] with scaling factors $\times 2$, $\times 3$, $\times 4$, $\times 6$, $\times 8$, $\times 12$. The best results are highlighted in red. The PSNR and SSIM [16] indices are computed in the Y channel of Ycbcr space.

| Scale | Metrics | Backbone: EDSR-baseline | | | | | | | | | | | | | | | | | |
|---|---|---|---|---|---|---|---|---|---|---|---|---|---|---|---|---|---|---|---|
| | | Testing Dataset: Set5 | | | | | | | | | Testing Dataset: Set14 | | | | | | | | |
| | | Meta -SR | LIIF | LTE | SRNO | LINF | LMF | Ciao -SR | Gaussian -SR | GSASR | Meta -SR | LIIF | LTE | SRNO | LINF | LMF | Ciao -SR | Gaussian -SR | GSASR |
| $\times 2$ | PSNR | 37.86 | 37.87 | 37.93 | 38.03 | 37.99 | 37.97 | 38.14 | 37.91 | 38.33 | 33.55 | 33.63 | 33.68 | 33.78 | 33.63 | 33.75 | 33.90 | 33.64 | 34.02 |
| | SSIM | 0.9603 | 0.9604 | 0.9604 | 0.9609 | 0.9605 | 0.9607 | 0.9610 | 0.9604 | 0.9619 | 0.9177 | 0.9186 | 0.9190 | 0.9201 | 0.9178 | 0.9196 | 0.9203 | 0.9189 | 0.9222 |
| | LPIPS | 0.0887 | 0.0549 | 0.0545 | 0.055 | 0.0564 | 0.0538 | 0.0542 | 0.0553 | 0.0517 | 0.0953 | 0.0943 | 0.0927 | 0.0920 | 0.0970 | 0.0916 | 0.0929 | 0.0936 | 0.0846 |
| | DISTS | 0.0819 | 0.0819 | 0.0827 | 0.0802 | 0.0814 | 0.0803 | 0.0797 | 0.0833 | 0.0766 | 0.0845 | 0.0839 | 0.0844 | 0.0830 | 0.0841 | 0.0829 | 0.0821 | 0.0845 | 0.0793 |
| $\times 3$ | PSNR | 34.31 | 34.35 | 34.39 | 34.47 | 34.45 | 34.52 | 34.49 | 34.39 | 34.84 | 30.27 | 30.32 | 30.35 | 30.47 | 30.33 | 30.41 | 30.46 | 30.34 | 30.65 |
| | SSIM | 0.9268 | 0.9273 | 0.9272 | 0.9282 | 0.9277 | 0.9285 | 0.9283 | 0.9276 | 0.9309 | 0.8421 | 0.8431 | 0.8437 | 0.8448 | 0.8430 | 0.8449 | 0.8450 | 0.8435 | 0.8498 |
| | LPIPS | 0.1276 | 0.1242 | 0.1243 | 0.1234 | 0.1261 | 0.1217 | 0.1211 | 0.1253 | 0.1209 | 0.2110 | 0.2067 | 0.2045 | 0.2038 | 0.2081 | 0.2005 | 0.2018 | 0.2056 | 0.1928 |
| | DISTS | 0.1292 | 0.1308 | 0.1324 | 0.1315 | 0.1299 | 0.1317 | 0.1284 | 0.1329 | 0.1291 | 0.1322 | 0.1311 | 0.1320 | 0.1303 | 0.1302 | 0.1297 | 0.1271 | 0.1327 | 0.1267 |
| $\times 4$ | PSNR | 32.04 | 32.20 | 32.20 | 32.35 | 32.26 | 32.30 | 32.42 | 32.22 | 32.79 | 28.51 | 28.60 | 28.63 | 28.74 | 28.62 | 28.69 | 28.77 | 28.62 | 28.88 |
| | SSIM | 0.8930 | 0.8955 | 0.8959 | 0.8974 | 0.8960 | 0.8967 | 0.8983 | 0.8958 | 0.9022 | 0.7808 | 0.7828 | 0.7836 | 0.7856 | 0.7826 | 0.7849 | 0.7865 | 0.7831 | 0.7902 |
| | LPIPS | 0.1768 | 0.1717 | 0.1733 | 0.1738 | 0.1757 | 0.1695 | 0.1688 | 0.1742 | 0.1686 | 0.2882 | 0.2832 | 0.2828 | 0.2790 | 0.2861 | 0.2794 | 0.2783 | 0.2849 | 0.2680 |
| | DISTS | 0.1559 | 0.1585 | 0.1585 | 0.158 | 0.1565 | 0.1596 | 0.1580 | 0.1586 | 0.1553 | 0.1636 | 0.1639 | 0.1637 | 0.1638 | 0.1642 | 0.1618 | 0.1615 | 0.1646 | 0.1574 |
| $\times 6$ | PSNR | 28.58 | 28.92 | 28.93 | 29.02 | 28.90 | 28.98 | 29.13 | 28.82 | 29.39 | 26.28 | 26.44 | 26.48 | 26.53 | 26.45 | 26.50 | 26.60 | 26.41 | 26.71 |
| | SSIM | 0.8204 | 0.8318 | 0.8311 | 0.8333 | 0.8314 | 0.8331 | 0.8357 | 0.8282 | 0.8418 | 0.6897 | 0.6964 | 0.6972 | 0.6989 | 0.6960 | 0.6968 | 0.7003 | 0.6936 | 0.7058 |
| | LPIPS | 0.2506 | 0.2406 | 0.2487 | 0.2471 | 0.2433 | 0.2470 | 0.2369 | 0.2484 | 0.2289 | 0.3957 | 0.3861 | 0.3919 | 0.3890 | 0.3900 | 0.3939 | 0.3823 | 0.3973 | 0.3731 |
| | DISTS | 0.2038 | 0.2009 | 0.204 | 0.2038 | 0.2020 | 0.2003 | 0.2014 | 0.2021 | 0.1964 | 0.2204 | 0.2197 | 0.2193 | 0.2184 | 0.2201 | 0.2195 | 0.2163 | 0.2221 | 0.2108 |
| $\times 8$ | PSNR | 26.69 | 26.96 | 27.02 | 27.05 | 26.95 | 27.07 | 27.16 | 26.77 | 27.33 | 24.75 | 24.92 | 24.96 | 25.03 | 24.92 | 25.00 | 25.09 | 24.80 | 25.23 |
| | SSIM | 0.7579 | 0.7764 | 0.777 | 0.7773 | 0.7763 | 0.7788 | 0.7829 | 0.7669 | 0.7863 | 0.6300 | 0.6395 | 0.6402 | 0.6456 | 0.6386 | 0.6403 | 0.6450 | 0.6330 | 0.6505 |
| | LPIPS | 0.3280 | 0.2993 | 0.3179 | 0.3152 | 0.3030 | 0.3092 | 0.2920 | 0.3198 | 0.2857 | 0.4674 | 0.4459 | 0.4593 | 0.4515 | 0.4526 | 0.4595 | 0.4395 | 0.4683 | 0.4359 |
| | DISTS | 0.2338 | 0.233 | 0.2376 | 0.238 | 0.2336 | 0.2381 | 0.2334 | 0.2396 | 0.2326 | 0.2578 | 0.2594 | 0.2595 | 0.2583 | 0.2589 | 0.2582 | 0.2541 | 0.2650 | 0.2480 |
| $\times 12$ | PSNR | 24.25 | 24.43 | 24.48 | 24.50 | 24.47 | 24.48 | 24.63 | 24.12 | 24.67 | 23.05 | 23.15 | 23.20 | 23.20 | 23.17 | 23.09 | 23.27 | 22.92 | 23.24 |
| | SSIM | 0.6656 | 0.6888 | 0.6883 | 0.6907 | 0.6884 | 0.6896 | 0.6985 | 0.6705 | 0.7055 | 0.5616 | 0.5738 | 0.5741 | 0.5758 | 0.5718 | 0.5706 | 0.5788 | 0.5621 | 0.5813 |
| | LPIPS | 0.4339 | 0.4129 | 0.4363 | 0.4257 | 0.4116 | 0.4220 | 0.4002 | 0.4586 | 0.3915 | 0.5587 | 0.5465 | 0.5638 | 0.5543 | 0.5476 | 0.5686 | 0.5340 | 0.5903 | 0.5306 |
| | DISTS | 0.2910 | 0.2922 | 0.2977 | 0.2986 | 0.2941 | 0.2947 | 0.2921 | 0.3072 | 0.2853 | 0.3078 | 0.3117 | 0.3162 | 0.3139 | 0.3138 | 0.3145 | 0.3091 | 0.3254 | 0.3049 |

Table 6. Quantitative results of representative ASR models and our proposed GSASR. All models use the same RDN backbone [22] as the feature extraction encoder. We test on Set5 [1] and Set14 [19] with scaling factors $\times 2$, $\times 3$, $\times 4$, $\times 6$, $\times 8$, $\times 12$. The best results are highlighted in red. The PSNR and SSIM [16] indices are computed in the Y channel of Ycbcr space.

| Scale | Metrics | Backbone: RDN | | | | | | | | | | | | | | | | | |
|---|---|---|---|---|---|---|---|---|---|---|---|---|---|---|---|---|---|---|---|
| | | Testing Dataset: Set5 | | | | | | | | | Testing Dataset: Set14 | | | | | | | | |
| | | Meta -SR | LIIF | LTE | SRNO | LINF | LMF | Ciao -SR | Gaussian -SR | GSASR | Meta -SR | LIIF | LTE | SRNO | LINF | LMF | Ciao -SR | Gaussian -SR | GSASR |
| $\times 2$ | PSNR | 38.24 | 38.07 | 38.11 | 38.2 | 38.21 | 38.13 | 38.32 | 38.13 | 38.38 | 34.03 | 33.92 | 34.04 | 34.21 | 33.93 | 34.07 | 34.23 | 34.06 | 34.16 |
| | SSIM | 0.9612 | 0.9611 | 0.9612 | 0.9617 | 0.9613 | 0.9613 | 0.9618 | 0.9612 | 0.9621 | 0.9207 | 0.9209 | 0.9213 | 0.9232 | 0.9206 | 0.9213 | 0.9226 | 0.9215 | 0.9226 |
| | LPIPS | 0.0536 | 0.0544 | 0.0538 | 0.0537 | 0.0549 | 0.0550 | 0.0538 | 0.0547 | 0.0510 | 0.0899 | 0.0892 | 0.0889 | 0.0879 | 0.0907 | 0.0895 | 0.0882 | 0.0902 | 0.0845 |
| | DISTS | 0.0798 | 0.0796 | 0.079 | 0.0786 | 0.0796 | 0.0790 | 0.0786 | 0.0797 | 0.0767 | 0.0812 | 0.0807 | 0.0803 | 0.0794 | 0.0812 | 0.0804 | 0.0794 | 0.0804 | 0.0788 |
| $\times 3$ | PSNR | 34.74 | 34.62 | 34.66 | 34.77 | 34.70 | 34.75 | 34.87 | 34.70 | 34.90 | 30.58 | 30.50 | 30.55 | 30.67 | 30.55 | 30.59 | 30.66 | 30.57 | 30.74 |
| | SSIM | 0.9296 | 0.9292 | 0.9297 | 0.9305 | 0.9296 | 0.9302 | 0.9306 | 0.9299 | 0.9313 | 0.8470 | 0.8470 | 0.8473 | 0.8492 | 0.8466 | 0.8483 | 0.8484 | 0.8475 | 0.8511 |
| | LPIPS | 0.1229 | 0.1234 | 0.1233 | 0.122 | 0.1228 | 0.1211 | 0.1215 | 0.1232 | 0.1208 | 0.2005 | 0.1988 | 0.1997 | 0.1993 | 0.2009 | 0.1973 | 0.1994 | 0.2004 | 0.1936 |
| | DISTS | 0.1312 | 0.1312 | 0.1303 | 0.1321 | 0.1300 | 0.1307 | 0.1299 | 0.1314 | 0.1283 | 0.1278 | 0.1272 | 0.1276 | 0.1260 | 0.1275 | 0.1271 | 0.1258 | 0.1282 | 0.1265 |
| $\times 4$ | PSNR | 32.51 | 32.47 | 32.56 | 32.64 | 32.49 | 32.56 | 32.68 | 32.55 | 32.83 | 28.85 | 28.77 | 28.84 | 28.93 | 28.82 | 28.87 | 28.94 | 28.82 | 28.96 |
| | SSIM | 0.8989 | 0.8989 | 0.8998 | 0.9008 | 0.8991 | 0.8998 | 0.9010 | 0.8994 | 0.9027 | 0.7882 | 0.7873 | 0.7888 | 0.7906 | 0.7879 | 0.7892 | 0.7906 | 0.7882 | 0.7922 |
| | LPIPS | 0.1712 | 0.1701 | 0.1708 | 0.1696 | 0.1721 | 0.1717 | 0.1689 | 0.1719 | 0.1688 | 0.2765 | 0.2766 | 0.2762 | 0.2744 | 0.2770 | 0.2763 | 0.2746 | 0.2786 | 0.2709 |
| | DISTS | 0.1556 | 0.1557 | 0.1558 | 0.157 | 0.1559 | 0.1580 | 0.1571 | 0.1575 | 0.1551 | 0.1588 | 0.1595 | 0.1590 | 0.1588 | 0.1590 | 0.1595 | 0.1581 | 0.1600 | 0.1573 |
| $\times 6$ | PSNR | 29.10 | 29.10 | 29.25 | 29.35 | 29.20 | 29.20 | 29.46 | 29.06 | 29.52 | 26.56 | 26.61 | 26.70 | 26.75 | 26.64 | 26.70 | 26.79 | 26.60 | 26.78 |
| | SSIM | 0.8326 | 0.8359 | 0.8367 | 0.8393 | 0.8362 | 0.8363 | 0.8415 | 0.8324 | 0.8441 | 0.6996 | 0.7027 | 0.7038 | 0.7061 | 0.7022 | 0.7042 | 0.7068 | 0.7002 | 0.7082 |
| | LPIPS | 0.2389 | 0.2344 | 0.2468 | 0.2433 | 0.2383 | 0.2461 | 0.2325 | 0.2457 | 0.2265 | 0.3782 | 0.3753 | 0.3849 | 0.3821 | 0.3810 | 0.3875 | 0.3757 | 0.3886 | 0.3724 |
| | DISTS | 0.1948 | 0.2011 | 0.2049 | 0.2015 | 0.2002 | 0.2016 | 0.1987 | 0.1998 | 0.1967 | 0.2104 | 0.2115 | 0.2127 | 0.2110 | 0.2136 | 0.2137 | 0.2100 | 0.2139 | 0.2096 |
| $\times 8$ | PSNR | 26.97 | 27.11 | 27.23 | 27.26 | 27.22 | 27.25 | 27.36 | 27.00 | 27.52 | 25.02 | 25.13 | 25.13 | 25.25 | 25.14 | 25.16 | 25.28 | 25.03 | 25.28 |
| | SSIM | 0.7692 | 0.7810 | 0.7828 | 0.7838 | 0.7833 | 0.7825 | 0.7877 | 0.7723 | 0.7937 | 0.6397 | 0.6464 | 0.6473 | 0.6503 | 0.6464 | 0.6468 | 0.6522 | 0.6412 | 0.6525 |
| | LPIPS | 0.3036 | 0.2918 | 0.3088 | 0.308 | 0.2956 | 0.3077 | 0.2871 | 0.3133 | 0.2788 | 0.4376 | 0.4347 | 0.4518 | 0.4482 | 0.4406 | 0.4526 | 0.4353 | 0.4555 | 0.4329 |
| | DISTS | 0.2252 | 0.2304 | 0.2348 | 0.2343 | 0.2300 | 0.2332 | 0.2311 | 0.2307 | 0.2285 | 0.2471 | 0.2506 | 0.2525 | 0.2502 | 0.2524 | 0.2535 | 0.2483 | 0.2552 | 0.2472 |
| $\times 12$ | PSNR | 24.49 | 24.69 | 24.66 | 24.77 | 24.70 | 24.67 | 24.83 | 24.24 | 24.68 | 23.18 | 23.22 | 23.30 | 23.32 | 23.28 | 23.28 | 23.41 | 23.02 | 23.27 |
| | SSIM | 0.6778 | 0.7011 | 0.6984 | 0.7019 | 0.6999 | 0.6965 | 0.7069 | 0.6769 | 0.7053 | 0.5680 | 0.5787 | 0.5807 | 0.5825 | 0.5779 | 0.5772 | 0.5848 | 0.5667 | 0.5834 |
| | LPIPS | 0.3952 | 0.3963 | 0.4272 | 0.4191 | 0.4063 | 0.4210 | 0.3920 | 0.4507 | 0.3813 | 0.5235 | 0.5302 | 0.5540 | 0.5418 | 0.5357 | 0.5576 | 0.5256 | 0.5761 | 0.5254 |
| | DISTS | 0.2775 | 0.2877 | 0.2926 | 0.2898 | 0.2901 | 0.2915 | 0.2882 | 0.2996 | 0.2820 | 0.2964 | 0.3053 | 0.3097 | 0.3053 | 0.3078 | 0.3104 | 0.3052 | 0.3163 | 0.3007 |

depends on the number of employed Gaussians. When inferring on ultra-high scaling factors, the representation capability will be limited if the number of Gaussians is insufficient. One way to handle this issue is to increase the number of Gaussians. Nonetheless, GSASR's results on $\times 12$ ASR are still very competitive.

## 2. Qualitative Results

We provide more qualitative results of our proposed GSASR and the compared methods, including Meta-SR [8], LIIF [3], LTE [10], SRNO [17], LINF [18], CiasoSR [2], LMF [6] and GaussianSR [7]. The visual comparisons are shown in Figure 1, 2, 3, 4, 5, 6, 7, 8. One could find that, GSASR generates much clearer details than all the other methods, especially for complex textures. For example, in Figure 1, the textures of the windows are very clear in GSASR, while the other methods lack lateral texture. Similar results could be observed from other visualization examples. In GSASR, Gaussians could move freely across the whole image, and automatically concentrate on areas with complex textures, benefiting the super-resolution of details. In the first row of Figure 9, one could find that Gaussians are inclined to concentrate more on the edge pixels, such as the building textures, while distributing uniformly on areas with smooth textures, such as the sky.

## 3. Computational Costs

We provide the computational costs of different ASR methods with RDN [22] as backbone. We report the average inference time (ms) and GPU memory (MB) usage on 100 images with $720 \times 720$ size that are cropped from DIV2K [15] dataset. The detailed results are shown in Table 7.

From Table 7, one could find that GSASR runs much faster than the SOTA method, CiaoSR [2], with comparable GPU memory usage on all scaling factors. When the scaling factor increases, GSASR could run with competitive speed with other methods, while keeping much better performance than all the other methods. For example, under the $\times 8$ scaling factor, the inference time of GSASR, LIIF [3], CiaoSR [2] is 206ms, 187ms, 633ms, respectively, while GSASR could still maintain a balanced performance. Advantaged by the efficient 2D GPU/CUDA-based rasterization, ours method could render a super-resolved image with high efficiency and fidelity.

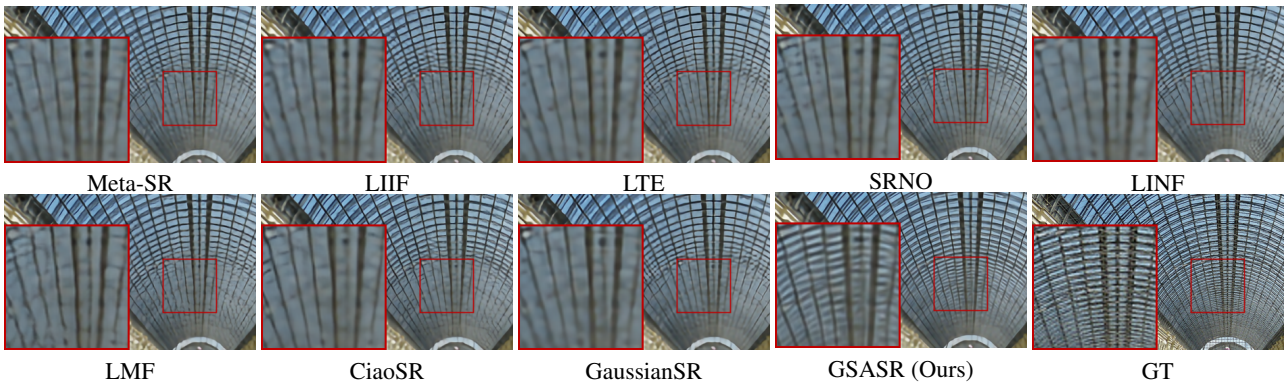


Figure 1. Visualization of GSASR and the competing methods under $\times 4$ scaling factor with EDSR [12] feature extraction backbone.

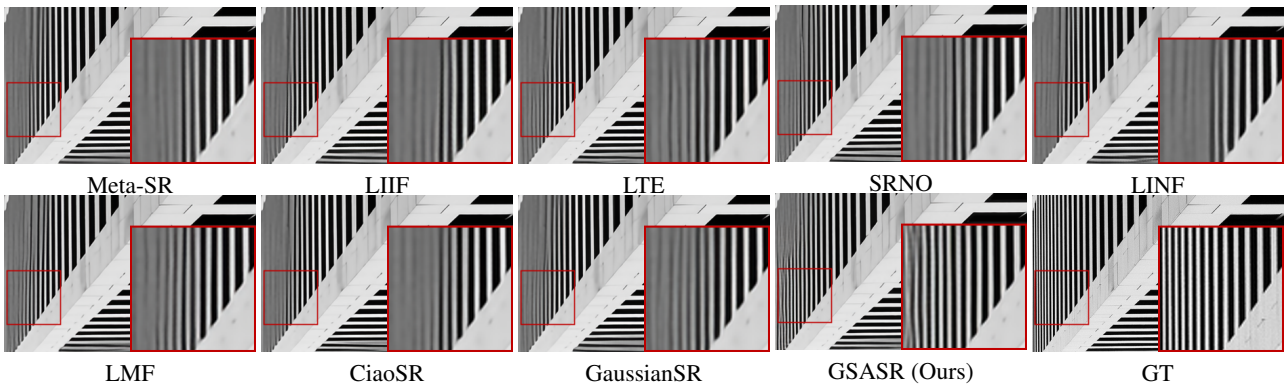


Figure 2. Visualization of GSASR and other methods under $\times 4$ scaling factor with RDN [22] feature extraction backbone.

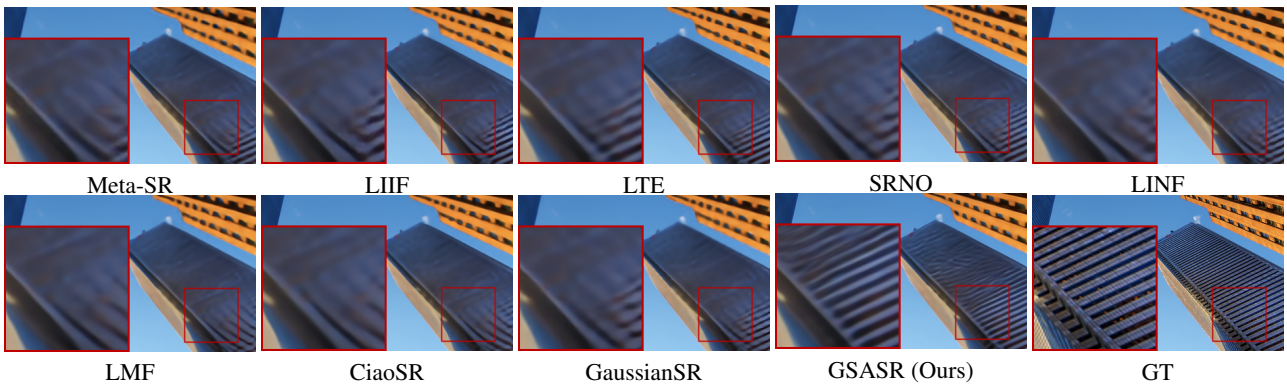


Figure 3. Visualization of GSASR and other methods under $\times 6$ scaling factor with EDSR [12] feature extraction backbone.

## 4. Ablation Study

We conduct ablation studies on two factors that affect the final performance of our proposed GSASR: 1) the total number of Gaussians $N$, and 2) the reference position.

### 4.1. Number of Gaussians

To study the effect of the number of Gaussians $N$ on super-resolution, we set the ratio of Gaussians to the corresponding LR image size ($H \times W$) to different values, $\frac{N}{HW} = \{1, 4, 9, 16\}$. The experiments are conducted on DIV2K [15]. The results are shown in Table 8. One could find that, with the increase of ratio $\frac{N}{HW}$, our method could obtain better super-resolution

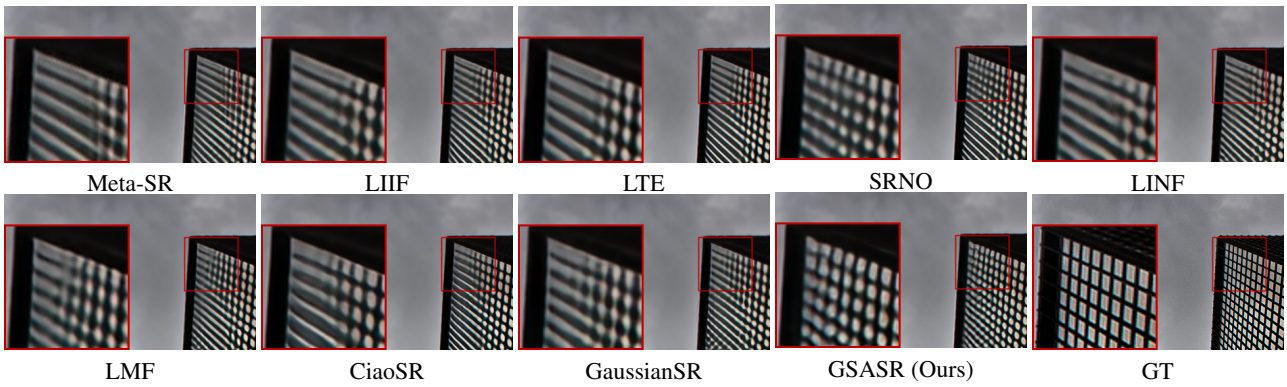


Figure 4. Visualization of GSASR and other methods under $\times 6$ scaling factor with RDN [22] feature extraction backbone.

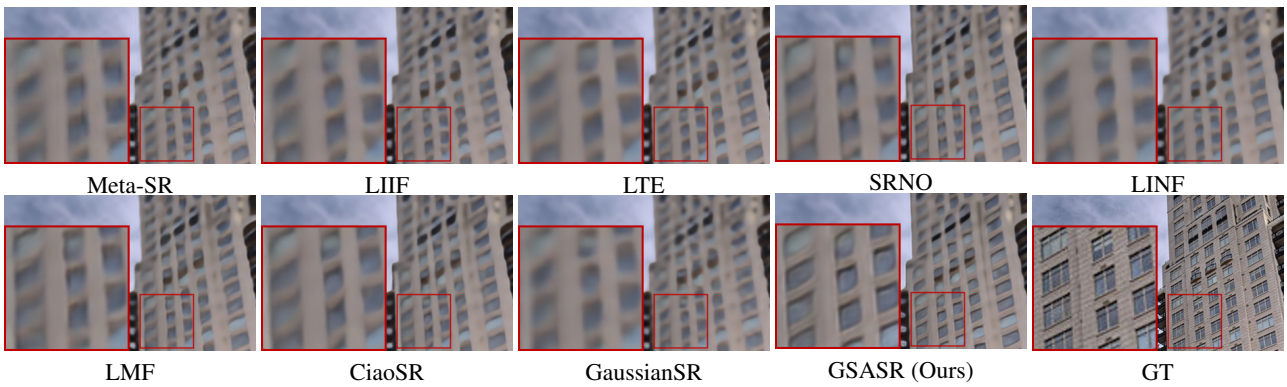


Figure 5. Visualization of GSASR and other methods under $\times 8$ scaling factor with EDSR [12] feature extraction backbone.

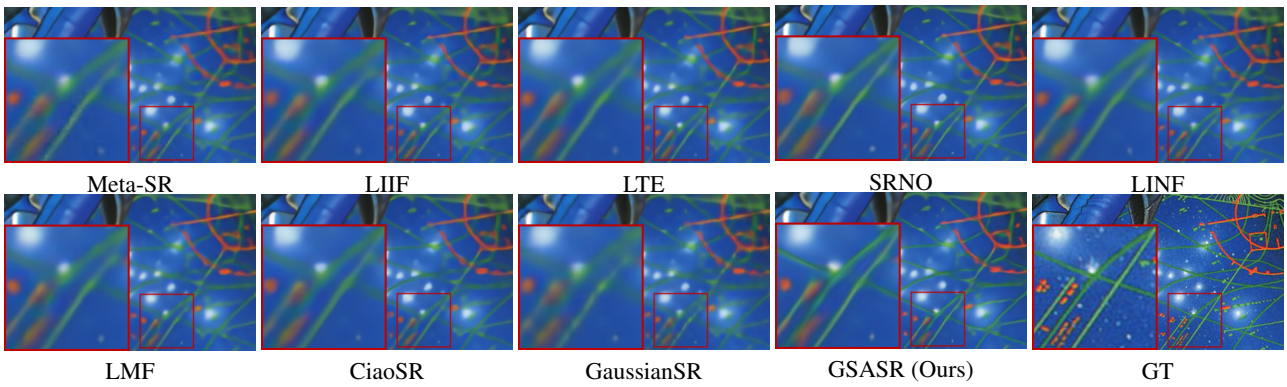


Figure 6. Visualization of GSASR and other methods under $\times 8$ scaling factor with RDN [22] feature extraction backbone.

results. Those phenomenons indicate that introducing more Gaussians could enhance the representation ability of our model. However, considering the computational cost, we set $\frac{N}{HW} = 16$ in default.

### 4.2. Reference Position

As discussed in the main paper, we assign a reference position $p_i$ to the $i$-th Gaussian embedding $E_i$, which predicts relative offset $o_i$ to obtain its final position with $\mu_i = p_i + o_i$. We provide the training loss curve comparison to demonstrate the importance of reference position. As shown in Figure 10, if we drop the reference position $p$ and make all Gaussian embeddings regress their final position $\mu$ directly, the training loss will not decrease and stop at around $4e^{-1}$. This is because the initial positions of the Gaussian embeddings lack differences, causing great difficulty in optimizing the network. In

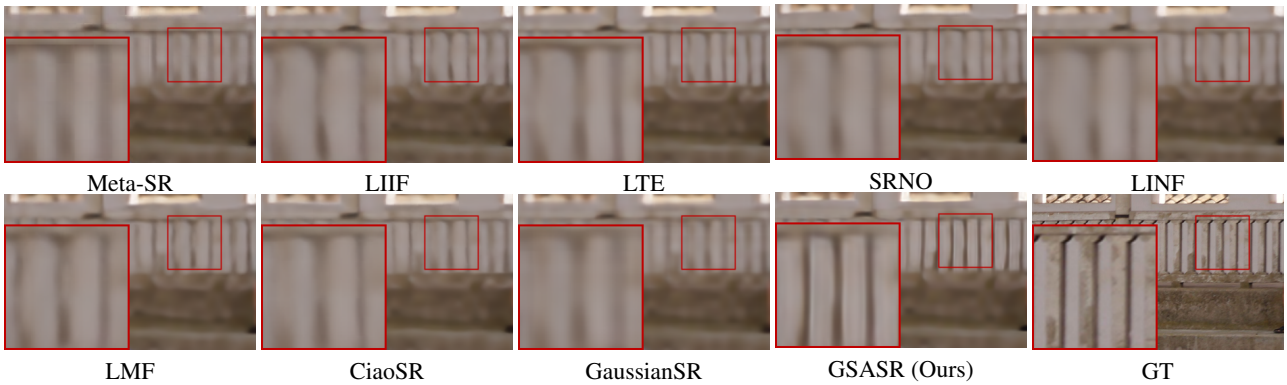


Figure 7. Visualization of GSASR and other methods under $\times 12$ scaling factor with EDSR [12] feature extraction backbone.

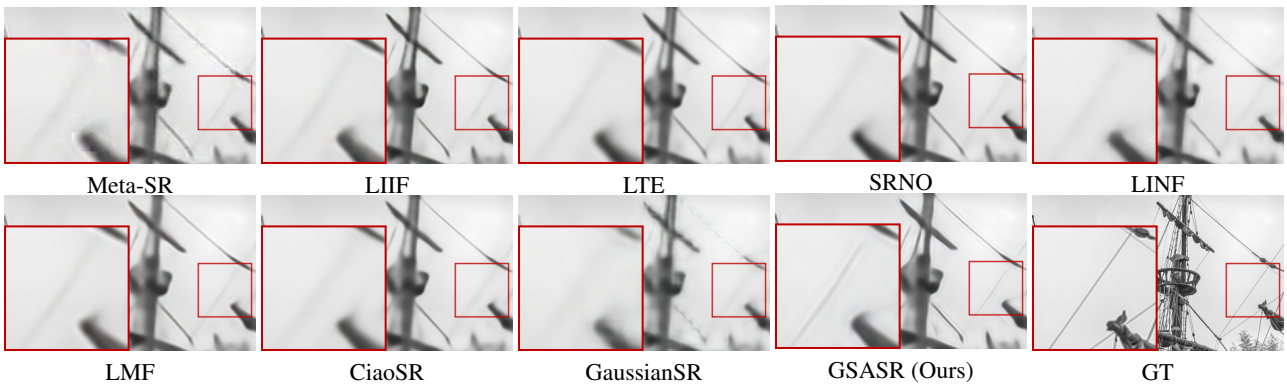


Figure 8. Visualization of GSASR and other methods under $\times 12$ scaling factor with RDN [22] feature extraction backbone.

contrast, introducing the reference position provides a desired initialization for the different Gaussian embeddings, so that the network can be properly optimized with loss decreasing to around $1e^{-2}$.

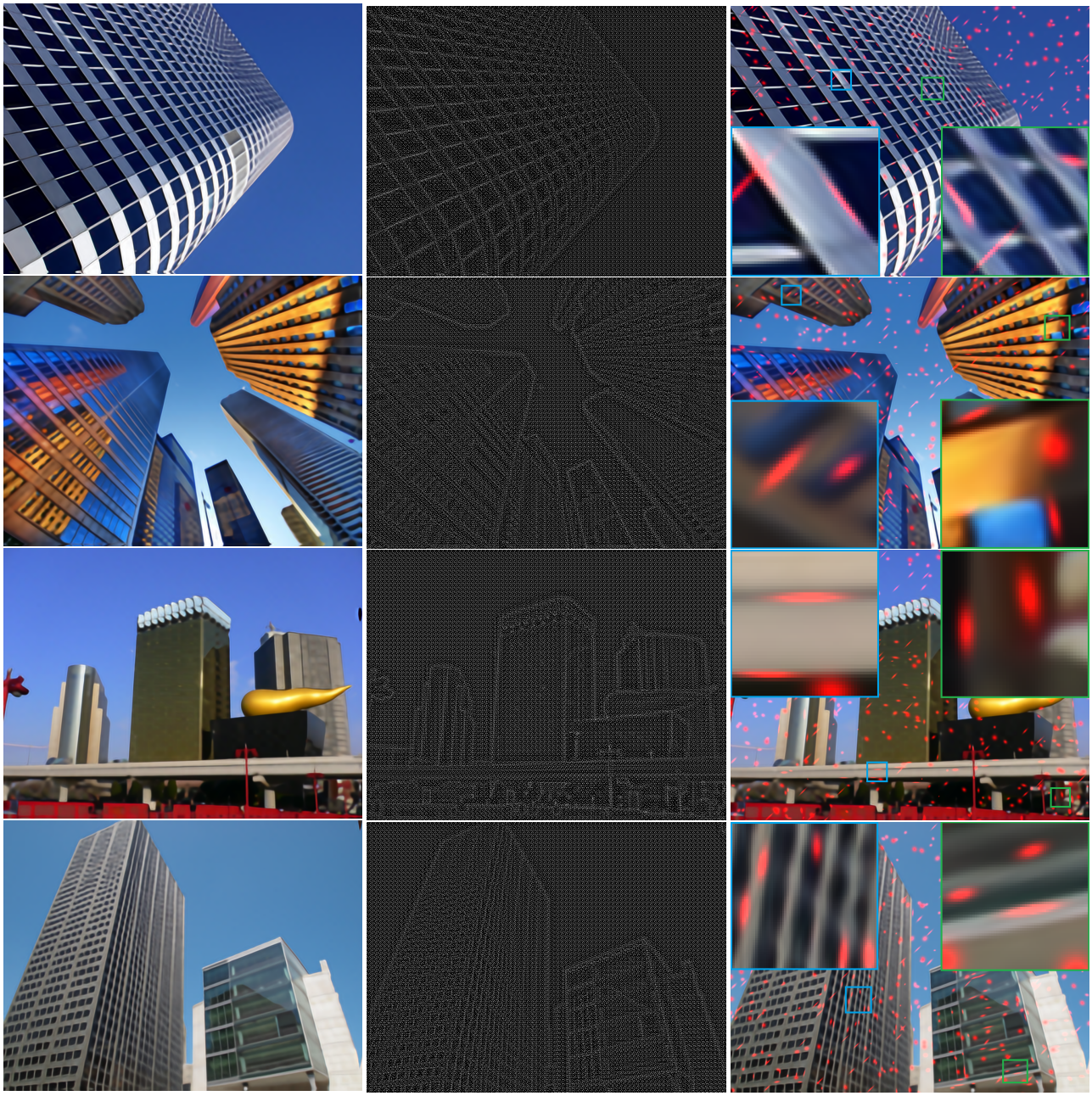

SR Image | Position Distribution of Gaussians | Colorized Gaussians

Figure 9. Demonstration of the rich expressiveness of Gaussians for ASR. The position distribution is obtained by setting $\{\sigma, \rho, c\}$ to fixed values. One can observe that Gaussians are evenly distributed in regions with simple textures, while their positions are adjusted in regions with complex textures to fit details. (**Please zoom in for better observation**.) In the right image, we randomly select parts of Gaussians and highlight their colors to red. One can see that 2D Gaussians can learn to fit the different object shapes ($e.g.$, the edge of window).

Table 7. Comparison of computational costs. We report the results using RDN [21] as image encoder. Apart from the PSNR/SSIM/LPIPS/DISTS metrics, we report the average inference time (ms) as well as the GPU memory (MB). The best results are highlighted in red.

| Scale | Computational Cost and Performance | Backbone: RDN | | | | | | | | |
|---|---|---|---|---|---|---|---|---|---|---|
| | | Testing GT Size: 720 * 720 | | | | | | | | |
| | | Meta-SR | LIIF | LTE | SRNO | LINF | LMF | CiaoSR | GaussianSR | GSASR |
| ×2 | PSNR | 37.76 | 37.41 | 37.44 | 37.64 | 37.74 | 37.61 | 37.85 | 37.54 | 37.92 |
| | SSIM | 0.9510 | 0.9509 | 0.9511 | 0.9521 | 0.9511 | 0.9515 | 0.9518 | 0.9512 | 0.9526 |
| | LPIPS | 0.0722 | 0.0734 | 0.0723 | 0.0695 | 0.0727 | 0.0715 | 0.0710 | 0.0735 | 0.0668 |
| | DISTS | 0.0709 | 0.0712 | 0.0703 | 0.0693 | 0.0706 | 0.0705 | 0.0687 | 0.0711 | 0.0670 |
| | Inference Time | 178 | 518 | 254 | 236 | 202 | 311 | 2381 | 1280 | 1679 |
| | GPU Memory | 8775 | 1246 | 1970 | 6381 | 3732 | 7096 | 49231 | 5278 | 13447 |
| ×3 | PSNR | 33.94 | 33.71 | 33.75 | 33.90 | 33.93 | 33.85 | 34.06 | 33.82 | 34.12 |
| | SSIM | 0.8979 | 0.8978 | 0.8982 | 0.8998 | 0.8981 | 0.8992 | 0.8996 | 0.8983 | 0.9015 |
| | LPIPS | 0.1692 | 0.1686 | 0.1678 | 0.1655 | 0.1687 | 0.1648 | 0.1667 | 0.169 | 0.1611 |
| | DISTS | 0.1224 | 0.1223 | 0.1206 | 0.1195 | 0.1221 | 0.1203 | 0.1180 | 0.1219 | 0.1172 |
| | Inference Time | 104 | 486 | 181 | 163 | 128 | 172 | 2064 | 955 | 857 |
| | GPU Memory | 8454 | 610 | 930 | 6361 | 3571 | 6108 | 10081 | 5216 | 6080 |
| ×4 | PSNR | 31.90 | 31.70 | 31.76 | 31.90 | 31.88 | 31.86 | 32.04 | 31.81 | 32.07 |
| | SSIM | 0.8505 | 0.8498 | 0.8508 | 0.8530 | 0.8503 | 0.8519 | 0.8531 | 0.8505 | 0.8549 |
| | LPIPS | 0.2399 | 0.2396 | 23.88 | 0.2350 | 0.2403 | 0.2380 | 0.2363 | 0.2403 | 0.2334 |
| | DISTS | 0.1585 | 0.1602 | 0.1585 | 0.1571 | 0.1604 | 0.1585 | 0.1572 | 0.1591 | 0.1528 |
| | Inference Time | 82 | 220 | 153 | 150 | 101 | 113 | 1202 | 824 | 572 |
| | GPU Memory | 8344 | 389 | 566 | 6354 | 3516 | 5764 | 3390 | 5130 | 3500 |
| ×6 | PSNR | 29.49 | 29.44 | 29.49 | 29.62 | 29.57 | 29.56 | 29.73 | 29.49 | 29.76 |
| | SSIM | 0.7782 | 0.7806 | 0.7814 | 0.7841 | 0.7806 | 0.7825 | 0.7848 | 0.7792 | 0.7867 |
| | LPIPS | 0.3274 | 0.3238 | 0.3317 | 0.3275 | 0.3296 | 0.3305 | 0.3217 | 0.3358 | 0.3210 |
| | DISTS | 0.2088 | 0.2129 | 0.2120 | 0.2105 | 0.2147 | 0.2119 | 0.2115 | 0.2129 | 0.2072 |
| | Inference Time | 69 | 201 | 136 | 118 | 84 | 94 | 736 | 751 | 284 |
| | GPU Memory | 8265 | 345 | 315 | 6350 | 3475 | 5517 | 1625 | 5301 | 1658 |
| ×8 | PSNR | 28.06 | 28.08 | 28.15 | 28.26 | 28.20 | 28.22 | 28.35 | 28.02 | 28.32 |
| | SSIM | 0.7305 | 0.7353 | 0.7366 | 0.7390 | 0.7350 | 0.7375 | 0.7400 | 0.7309 | 0.7414 |
| | LPIPS | 0.3877 | 0.3816 | 0.3958 | 0.3910 | 0.3911 | 0.3946 | 0.3814 | 0.4039 | 0.3799 |
| | DISTS | 0.2425 | 0.2489 | 0.2500 | 0.2477 | 0.2514 | 0.2499 | 0.2478 | 0.2521 | 0.2433 |
| | Inference Time | 55 | 187 | 128 | 107 | 77 | 80 | 633 | 702 | 206 |
| | GPU Memory | 8236 | 328 | 302 | 6348 | 3462 | 5431 | 1583 | 5092 | 1132 |
| ×12 | PSNR | 26.25 | 26.33 | 26.41 | 26.49 | 26.42 | 26.44 | 26.56 | 26.08 | 26.58 |
| | SSIM | 0.6746 | 0.6828 | 0.6838 | 0.6857 | 0.6817 | 0.6842 | 0.6875 | 0.6737 | 0.6884 |
| | LPIPS | 0.4716 | 0.4701 | 0.4896 | 0.4845 | 0.4837 | 0.4868 | 0.4691 | 0.5162 | 0.4665 |
| | DISTS | 0.2935 | 0.3022 | 0.3062 | 0.3038 | 0.3071 | 0.3060 | 0.3019 | 0.3141 | 0.2983 |
| | Inference Time | 58 | 178 | 129 | 114 | 78 | 110 | 546 | 701 | 98 |
| | GPU Memory | 8216 | 317 | 293 | 6347 | 3451 | 5369 | 1549 | 5291 | 553 |

Table 8. Ablation study on the number of Gaussians $N$. We utilize the EDSR-backbone [12] to extract the deep feature. DIV2K [15] dataset is utilized as the testing set. The best results are highlighted in red.

| The Value of Ratio $\frac{N}{HW}$ | Backbone: EDSR-baseline | | | | | | | | | | | |
|---|---|---|---|---|---|---|---|---|---|---|---|---|
| | Testing Datasets: DIV2K | | | | | | | | | | | |
| | ×2 | | | | ×4 | | | | ×6 | | | |
| | PSNR | SSIM | LPIPS | DISTS | PSNR | SSIM | LPIPS | DISTS | PSNR | SSIM | LPIPS | DISTS |
| 1 | 36.56 | 0.9487 | 0.0772 | 0.0528 | 30.75 | 0.8461 | 0.2603 | 0.1328 | 28.45 | 0.7760 | 0.3521 | 0.1888 |
| 4 | 36.63 | 0.9490 | 0.0771 | 0.0520 | 30.82 | 0.8477 | 0.2544 | 0.1317 | 28.49 | 0.7773 | 0.3477 | 0.1862 |
| 9 | 36.64 | 0.9494 | 0.0767 | 0.0516 | 30.86 | 0.8482 | 0.2523 | 0.1303 | 28.56 | 0.7783 | 0.3438 | 0.1840 |
| 16 | 36.65 | 0.9495 | 0.0767 | 0.0514 | 30.89 | 0.8486 | 0.2518 | 0.1301 | 28.60 | 0.7784 | 0.3435 | 0.1835 |

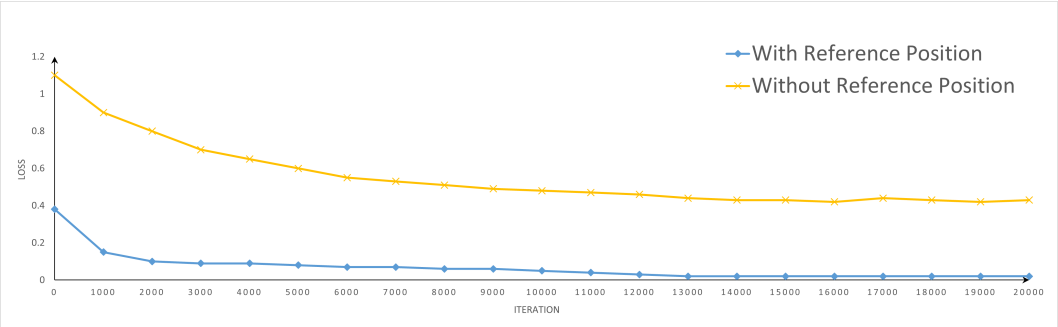


Figure 10. The training loss curves with and without reference position.

## References


[1] Marco Bevilacqua, Aline Roumy, Christine Guillemot, and Marie Line Alberi-Morel. Low-complexity single-image super-resolution based on nonnegative neighbor embedding. In *BMVC*, pages 135.1–135.10, 2012. 1, 3, 4

[2] Jiezhang Cao, Qin Wang, Yongqin Xian, Yawei Li, Bingbing Ni, Zhiming Pi, Kai Zhang, Yulun Zhang, Radu Timofte, and Luc Van Gool. Ciaosr: Continuous implicit attention-in-attention network for arbitrary-scale image super-resolution. In *Proceedings of the IEEE/CVF Conference on Computer Vision and Pattern Recognition*, pages 1796–1807, 2023. 1, 4

[3] Yinbo Chen, Sifei Liu, and Xiaolong Wang. Learning continuous image representation with local implicit image function. In *IEEE Conference on Computer Vision and Pattern Recognition*, pages 8628–8638, 2021. 1, 4

[4] Keyan Ding, Kede Ma, Shiqi Wang, and Eero P Simoncelli. Image quality assessment: Unifying structure and texture similarity. *IEEE Transactions on Pattern Analysis and Machine Intelligence*, 44(5):2567–2581, 2020. 1

[5] Chao Dong, Chen Change Loy, and Xiaoou Tang. Accelerating the super-resolution convolutional neural network. In *European Conference on Computer Vision*, pages 391–407. Springer, 2016. 1, 2, 3

[6] Zongyao He and Zhi Jin. Latent modulated function for computational optimal continuous image representation. In *Proceedings of the IEEE/CVF Conference on Computer Vision and Pattern Recognition*, pages 26026–26035, 2024. 1, 4

[7] Jintong Hu, Bin Xia, Bin Chen, Wenming Yang, and Lei Zhang. Gaussiansr: High fidelity 2d gaussian splatting for arbitrary-scale image super-resolution. In *Proceedings of the Association for the Advancement of Artificial Intelligence*, 2025. 1, 4

[8] Xuecai Hu, Haoyuan Mu, Xiangyu Zhang, Zilei Wang, Tieniu Tan, and Jian Sun. Meta-sr: A magnification-arbitrary network for super-resolution. In *IEEE Conference on Computer Vision and Pattern Recognition*, pages 1575–1584, 2019. 1, 4

[9] Jia-Bin Huang, Abhishek Singh, and Narendra Ahuja. Single image super-resolution from transformed self-exemplars. In *IEEE Conference on Computer Vision and Pattern Recognition*, pages 5197–5206, 2015. 1, 2

[10] Jaewon Lee and Kyong Hwan Jin. Local texture estimator for implicit representation function. In *Proceedings of the IEEE/CVF Conference on Computer Vision and Pattern Recognition*, pages 1929–1938, 2022. 1, 4

[11] Yawei Li, Kai Zhang, Jingyun Liang, Jiezhang Cao, Ce Liu, Rui Gong, Yulun Zhang, Hao Tang, Yun Liu, Denis Demandolx, et al. Lsdir: A large scale dataset for image restoration. In *Proceedings of the IEEE/CVF Conference on Computer Vision and Pattern Recognition*, pages 1775–1787, 2023. 1

[12] Bee Lim, Sanghyun Son, Heewon Kim, Seungjun Nah, and Kyoung Mu Lee. Enhanced deep residual networks for single image super-resolution. In *IEEE Conference on Computer Vision and Pattern Recognition Workshop*, pages 136–144, 2017. 1, 2, 3, 5, 6, 7, 9

[13] David Martin, Charless Fowlkes, Doron Tal, and Jitendra Malik. A database of human segmented natural images and its application to evaluating segmentation algorithms and measuring ecological statistics. In *IEEE International Conference on Computer Vision*, pages 416–423. IEEE, 2001. 1, 2, 3

[14] Yusuke Matsui, Kota Ito, Yuji Aramaki, Azuma Fujimoto, Toru Ogawa, Toshihiko Yamasaki, and Kiyoharu Aizawa. Sketch-based manga eetrieval using manga109 dataset. *Multimedia Tools and Applications*, 76(20):21811–21838, 2017. 1, 2

[15] Radu Timofte, Eirikur Agustsson, Luc Van Gool, Ming-Hsuan Yang, and Lei Zhang. Ntire 2017 challenge on single image super-resolution: Methods and results. In *IEEE Conference on Computer Vision and Pattern Recognition Workshop*, pages 114–125, 2017. 1, 4, 5, 9

[16] Zhou Wang, Alan C Bovik, Hamid R Sheikh, and Eero P Simoncelli. Image quality assessment: From error visibility to structural similarity. *IEEE Transactions on Image Processing*, 13(4):600–612, 2004. 1, 2, 3, 4

[17] Min Wei and Xuesong Zhang. Super-resolution neural operator. In *Proceedings of the IEEE/CVF Conference on Computer Vision and Pattern Recognition*, pages 18247–18256, 2023. 1, 4

[18] Jie-En Yao, Li-Yuan Tsao, Yi-Chen Lo, Roy Tseng, Chia-Che Chang, and Chun-Yi Lee. Local implicit normalizing flow for arbitrary-scale image super-resolution. In *Proceedings of the IEEE/CVF Conference on Computer Vision and Pattern Recognition*, pages 1776–1785, 2023. 1, 4

[19] Roman Zeyde, Michael Elad, and Matan Protter. On single image scale-up using sparse-representations. In *International Conference on Curves and Surfaces*, pages 711–730. Springer, 2010. 1, 3, 4

[20] Richard Zhang, Phillip Isola, Alexei A Efros, Eli Shechtman, and Oliver Wang. The unreasonable effectiveness of deep features as a perceptual metric. In *IEEE Conference on Computer Vision and Pattern Recognition*, pages 586–595, 2018. 1

[21] Yulun Zhang, Kunpeng Li, Kai Li, Lichen Wang, Bineng Zhong, and Yun Fu. Image super-resolution using very deep residual channel attention networks. In *European Conference on Computer Vision*, pages 286–301, 2018. 2, 9

[22] Yulun Zhang, Yapeng Tian, Yu Kong, Bineng Zhong, and Yun Fu. Residual dense network for image super-resolution. In *IEEE Conference on Computer Vision and Pattern Recognition*, pages 2472–2481, 2018. 3, 4, 5, 6, 7